Electronic Supplementary Information

Tritopic ion-pair receptors based on anion-π interactions for selective CaX_2 binding

Jian Luo,[a,b] Yu-Fei Ao,[a] Christian Malm,[c] Johannes Hunger,[c] Qi-Qiang Wang,[*,a,b] De-Xian Wang[*,a,b]

[a] Beijing National Laboratory for Molecular Sciences, CAS Key Laboratory of Molecular Recognition and Function, Institute of Chemistry, Chinese Academy of Sciences, Beijing, 100190, China.

[b] University of Chinese Academy of Sciences, Beijing 100049, China.

[c] Molecular Spectroscopy Department, Max Planck Institute for Polymer Research, Ackermannweg 10, 55128 Mainz, Germany

Contents

1. General methods

All chemicals were obtained from commercial sources and used without further purification unless stated otherwise. NMR spectra were recorded on Bruker 400 or 500 MHz NMR spectrometer at room temperature. Chemical shifts are reported in ppm and referenced to tetramethylsilane or the residual solvent resonance. Mass spectra were obtained on a Thermo Fisher Exactive Mass Spectrometer. Infrared spectra were recorded using a Nicolet-6700 FT-IR spectrometer with KBr pellets in the 4000-400 cm^{-1} region. Elemental analysis was recorded on Thermo Quest CE Instruments flash EA 1112 analyser. Melting points are uncorrected.

2. Syntheses and characterization

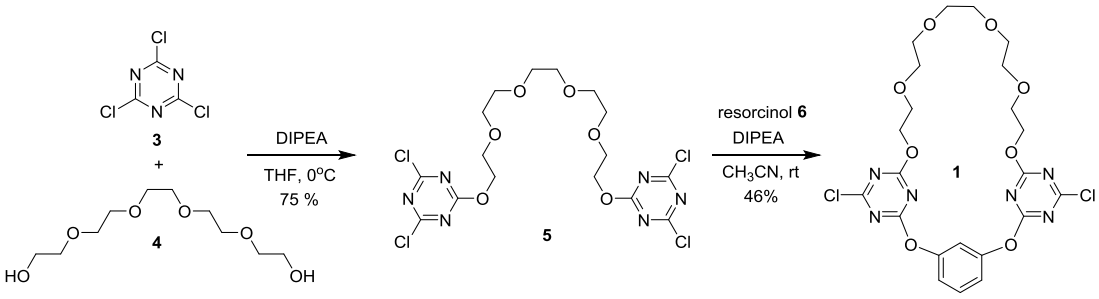

Scheme S1. Synthesis of macrocycle **1**.

Synthesis of 5. To a solution of cyanuric chloride **3** (40.00 g, 217 mmol) in 200 mL THF, pentaethylene glycol **4** (23.80 g, 100 mmol) and DIPEA (diisopropylethylamine, 38 mL, 218 mmol) in 200 mL THF were added dropwise under ice-bath during a period of 2 hours. The mixture was kept stirring for 6 hours under ice bath. After the reaction was finished, solvent was removed by a rotary evaporator in vacuo. The residue was chromatographed by silica gel (100-200 mesh) with a mixture of ethyl acetate and petroleum ether (3:7, v/v) as the eluent to yield **5** (40.10 g, 75.1 mmol, 75%) as faint yellow oil.

5: Oil; IR (KBr) ν 2874, 1558, 1516, 1480, 1439, 1345, 1307, 1256, 1178, 1138, 1058, 943, 876, 841, 806; ^{1}H NMR (500 MHz, $CDCl_3$): δ 4.66 (t, *J* = 4.6 Hz, 4H), 3.87 (t, *J* = 4.6 Hz, 4H), 3.70-3.68 (m, 12H); ^{13}C NMR (125 MHz, $CDCl_3$): δ 172.47, 171.04,

70.82, 70.62, 70.57, 69.36, 68.41; HR-ESI-MS (positive mode): *m/z* $[M+Na]^+$ calcd. 557.0061; Found: 557.0061; Anal. Clacd (%) for $C_{16}H_{20}Cl_4N_6O_6$: C, 35.98; H, 3.77; N, 15.74; Found: C, 36.17; H, 3.86; N, 15.48.

Synthesis of 1. **5** (5.34 g, 10 mmol) and resorcinol **6** (1.10 g, 10 mmol) were dissolved in 500 mL acetonitrile. To this solution was added dropwise DIPEA (4.2 mL, 24 mmol) in 250 mL acetonitrile during a period of 2 hours and then kept stirring for 4 hours. Solvent was removed in vacuo by a rotary evaporator. The residue was chromatographed on silica gel (100-200 mesh) with a mixture of dichloromethane and acetone (9:1, v/v) as eluent to yield **1** (2.64 g, 4.6 mmol, 46%) as a white solid.

1: mp 123-124 °C; IR (KBr) ν 2919, 1602, 1569, 1539, 1483, 1443, 1394, 1340, 1297, 1243, 1214, 1138, 1103, 1027, 991, 812; ^{1}H NMR (500 MHz, $CDCl_3$): δ 7.49 (t, *J* = 8.3 Hz, 1H), 7.19 (t, *J* = 2.2 Hz, 1H), 7.13 (dd, *J* = 8.3 Hz, 2.2 Hz, 2H), 4.51 (t, *J* = 4.5 Hz, 4H), 3.78 (t, *J* = 4.6 Hz, 4H), 3.61-3.58 (m, 8H), 3.57 (s, 4H); ^{13}C NMR (125 MHz, CD_3CN): δ 173.80, 173.38, 173.12, 153.08, 131.68, 120.58, 116.55, 71.34, 71.27, 71.25, 69.62, 69.22; HR-APCI-MS (positive mode) *m/z*: $[M+H]^+$ calcd for $C_{22}H_{25}Cl_2N_6O_8$: 571.1105, Found: 571.1091; Anal. Clacd(%) for $C_{22}H_{24}Cl_2N_6O_8$: C, 46.25; H, 4.23; N, 14.71; Found: C, 46.17; H, 4.24; N, 14.75.

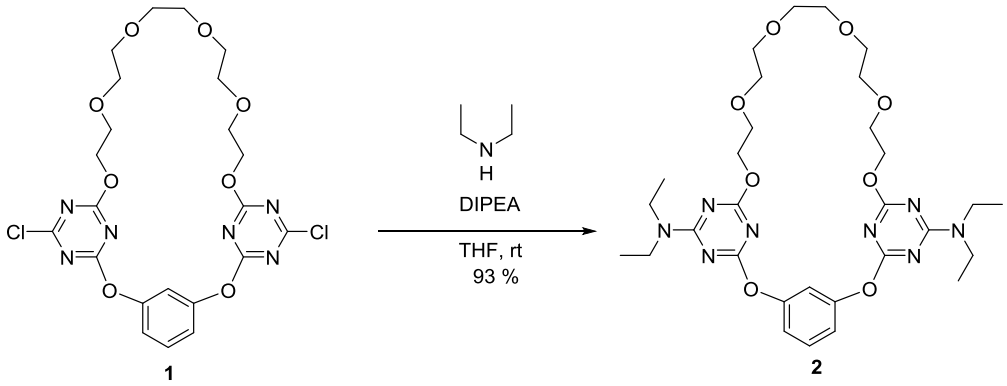

Scheme S2. Synthesis of **2**

Synthesis of 2: Macrocycle **1** (571 mg, 1 mmol), diethylamine (219 mg, 3 mmol), and DIPEA (1.03 g, 8 mmol) were dissolved in 100 mL THF and stirred for 5 hours. Then the solvent was removed in vacuo by rotary evaporator. The residue was chromatographed on silica gel (100-200 mesh) with a mixture of petroleum ether and acetone (3:1, v/v) as eluent to yield **2** (600 mg, 0.93 mmol, 93%) as colorless oil.

2: IR (KBr) ν 2973, 2935, 2873, 1594, 1528, 1483, 1464, 1423, 1362, 1318, 1268, 1213, 1141, 1105, 945, 814; ^{1}H NMR (500 MHz, $CDCl_3$): δ 7.35 (t, *J* = 8.2 Hz, 1H), 7.12 (t, *J* = 2.0 Hz, 1H), 7.04 (dd, *J* = 8.2 Hz, 2.0 Hz, 2H), 4.39 (t, *J* = 4.7 Hz, 4H), 3.75 (t, *J* = 4.8 Hz, 4H), 3.62-3.55 (m, 20H), 1.20-1.15 (m, 12H); ^{13}C NMR (125 MHz, CD_3CN): δ 172.85, 172.67, 167.68, 153.86, 130.45, 119.66, 116.93, 71.31, 71.29, 69.82, 67.43, 42.80, 42.71, 13.34; HR-APCI-MS (positive mode) *m/z*: $[M+H]^+$ calcd for $C_{30}H_{45}N_8O_8$: 645.3355, Found: 645.3371; Anal. Clacd (%) for $C_{30}H_{44}N_8O_8$: C, 55.89; H, 6.88; N, 17.38; Found: C, 55.73; H, 6.82; N, 17.41.

3. X-Ray diffraction data

Procedures for cultivation of single crystals.

1:

Method (A), 2 mg **1** was dissolved in 2 mL methanol, ethyl ether was allowed to slowly diffuse into the solution at 273 K, colorless crystal was obtained after 2 days.

Method (B), 2 mg **1** was dissolved in 2 mL acetone, about 0.5 mL water was added into the solution, it was allowed to slowly evaporate for 2 days at room temperature to obtain colorless crystal.

Method (A) and (B) afford different single crystals.

1·$CaBr_2$:

Method (A), 3 mg **1**, 4 mg $Ca(ClO_4)_2 \cdot 4H_2O$ and 8 mg NBu_4Br were dissolved in 2 mL acetonitrile (contain one drop of methanol), ethyl ether was allowed to slowly diffuse into the solution at 273 K, colorless single crystal was obtained after 2 days.

Method (B), 3 mg **1** and 3 mg $CaBr_2$ were dissolved in 2 mL acetonitrile (contain one drop of methanol), ethyl ether was allowed to slowly diffuse into the solution at 273 K, colorless single crystal was obtained after 2 days.

Method (A) and (B) afford same single crystals.

1·CaI_2:

Method (A), 3 mg **1**, 4 mg $Ca(ClO_4)_2 \cdot 4H_2O$ and 8 mg NBu_4I were dissolved in 2 mL acetonitrile, ethyl ether was allowed to slowly diffuse into the solution at 273 K, colorless single crystal was obtained after 2 days.

Method (B), 3 mg **1** and 4 mg CaI_2 were dissolved in 2 mL acetonitrile, ethyl ether was allowed to slowly diffuse into the solution at 273 K, colorless single crystal was obtained after 2 days.

Method (A) and (B) afford the same single crystals.

Single crystal X-ray diffraction data were collected on a MM007HF Saturn724+ diffractometer using MoK/α radiation (λ=0.71073 Å) at a temperature of 173 K. The intensity data were collected by the omega scans techniques, scaled, and reduced with CrystalClear (Rigaku Inc., 2007). X-rays were provided by a fine-focus sealed X-ray tube operated at 50 kV and 24 mA.

Integrated reflection intensities were produced and the correction of the collected intensities for absorption was done using the CrystalClear (Rigaku Inc., 2007) program. The structure were solved by direct methods using SHELXT (Sheldrick, 2014) and refined using full-matrix least-squares methods in ShelXL (Sheldrick, 2014/2015). All non-hydrogen atoms were refined anisotropically, and hydrogen atos attached to carbon atoms were fixed at their ideal positions.

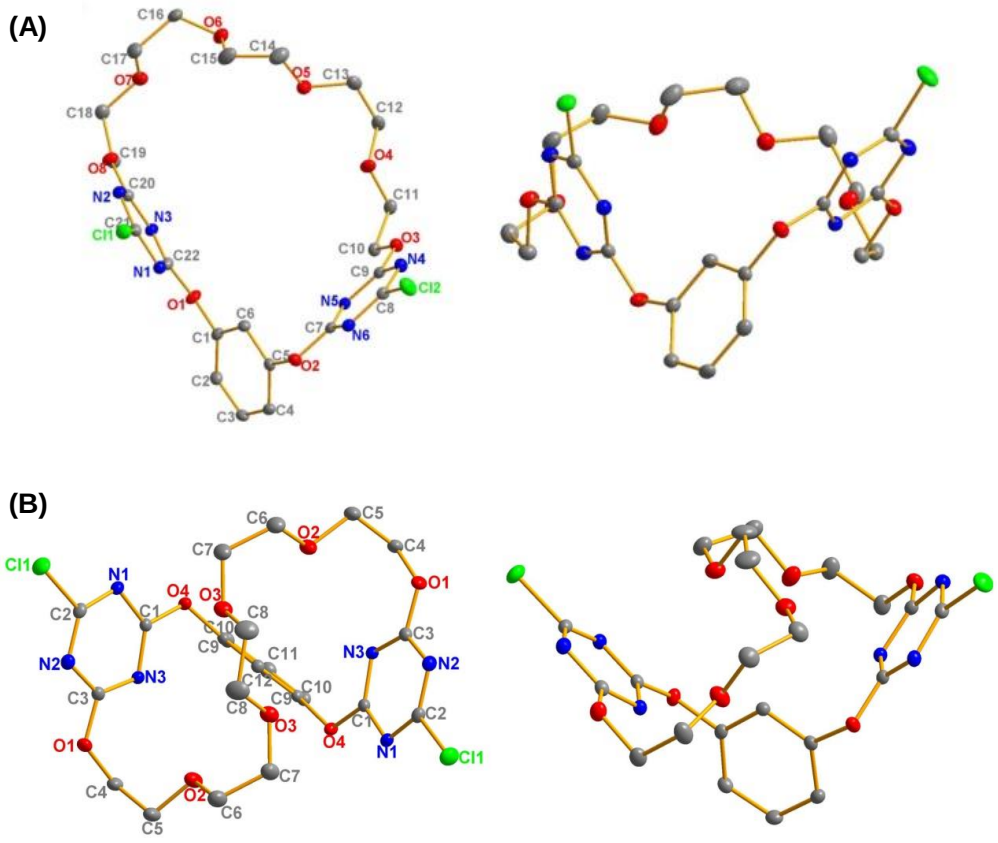

Figure S1. Crystal structures of **1**. (A), the crystal was obtained by slow diffusion of ethyl ether into a solution in methanol. (B), the crystal was obtained by slow evaporation of a solution in acetone/water. Hydrogen atoms are omitted for clarity.

Table S1. Crystal data and structure refinement for **1**

	1(A)	**1**(B)
CCDC number.	1833035	1833036
Empirical formula	C22 H24 Cl2 N6 O8	C22 H24 Cl2 N6 O8
Formula weight	571.37	571.37
Temperature	173.15 K	173.15 K
Wavelength	0.710747 Å	0.71073 Å
Crystal system	Triclinic	Monoclinic
Space group	P -1	C 1 2/c 1
A	9.0185(10) Å	11.245(2) Å
B	11.602(2) Å	17.678(3) Å
C	13.015(3) Å	13.048(2) Å
A	70.854(3) °	90 °
B	81.101(2) °	95.709(2) °
Γ	89.578(3) °	90 °
Volume	1269.6(4) $Å^3$	2580.7(8) $Å^3$
Z	2	4
Density(calculated)	1.495 Mg/m^3	1.471 Mg/m^3
Absorption coefficient	0.315 mm^{-1}	0.310 mm^{-1}
F(000)	592	1184
Crystal size	0.15 x 0.04 x 0.03 mm^3	0.267 x 0.184 x 0.102 mm^3
Theta range for data collected	2.288 to 27.474 °	2.154 to 27.483 °.
Index ranges	-7<=h<=11, -15<=k<=15, -16<=l<=16	-13<=h<=14, -22<=k<=22, -16<=l<=16
Reflections collected	11556	10750
Independent reflections	5684 [R(int) = 0.0319]	2953 [R(int) = 0.0292]
Completeness to theta=25.242 °	9810.00 %	99.4 %
Absorption correction	Semi-empirical from equivalents	Semi-empirical from equivalents
Max. and min. transmission	1.0000 and 0.8165	1.0000 and 0.8544
Refinement method	Full-matrix least-squares on F^2	Full-matrix least-squares on F^2
Data/restraints/parameters	5684 / 0 / 343	2953 / 0 / 173
Goodness-of-fit on F^2	1.079	1.096
Final R indices (all data)	R1 = 0.0478, wR2 = 0.0954	R1 = 0.0468, wR2 = 0.1167
R indices (all data)	R1 = 0.0557, wR2 = 0.1002	R1 = 0.0489, wR2 = 0.1184
Extinction coefficient	n/a	n/a
Largest diff. peak and hole	0.380 and -0.438 e.$Å^{-3}$	0.674 and -0.252 e.$Å^{-3}$

Table S2. Crystal data and structure refinement for **1** CaI_2 and **1** $CaBr_2$

	1·$CaBr_2$·CH_3OH·H_2O	**1**·CaI_2·$2H_2O$·$2CH_3CN$
CCDC number.	1833037	1833038
Empirical formula	C23 H30 Br2 Ca Cl2 N6 O10	C26 H34 Ca Cl2 I2 N8 O10
Formula weight	821.33	983.39
Temperature	173.15 K	173(2) K
Wavelength	0.71073 Å	0.71073 Å
Crystal system	Monoclinic	Orthorhombic
Space group	P 1 21/c 1	$Pna2_1$
A	18.081(4) Å	17.615(3) Å
B	7.8133(15) Å	15.703(3) Å
C	23.448(5) Å	13.956(2) Å
A	90 °	90 °
B	103.521(2) °	90 °
Γ	90 °	90 °
Volume	3220.7(11) $Å^3$	3860.6(11) $Å^3$
Z	4	4
Density(calculated)	1.694 Mg/m^3	1.692 Mg/m^3
Absorption coefficient	2.903 mm^{-1}	1.959 mm^{-1}
F(000)	1656	1944
Crystal size	0.232 x 0.166 x 0.147 mm^3	0.365 x 0.356 x 0.175 mm^3
Theta range for data collected	1.888 to 27.498 °	1.737 to 27.476 °.
Index ranges	-23<=h<=23, -10<=k<=9, -30<=l<=30	-22<=h<=20, -12<=k<=20, -12<=l<=18
Reflections collected	21205	13046
Independent reflections	7261 [R(int) = 0.0320]	7276 [R(int) = 0.0576]
Completeness to theta=25.242 °	98.8 %	99.3 %
Absorption correction	Semi-empirical from equivalents	Semi-empirical from equivalents
Max. and min. transmission	1.0000 and 0.7606	1.000 and 0.781
Refinement method	Full-matrix least-squares on F^2	Full-matrix least-squares on F^2
Data/restraints/parameters	7261 / 3 / 404	7276 / 1 / 173(2)
Goodness-of-fit on F^2	1.078	1.060
Final R indices (all data)	R1 = 0.0365, wR2 = 0.0873	R1 = 0.0448, wR2 = 0.1116
R indices (all data)	R1 = 0.0405, wR2 = 0.0903	R1 = 0.0474, wR2 = 0.1148
Extinction coefficient	n/a	n/a
Absolute structure parameter		-0.02(3)
Largest diff. peak and hole	1.189 and -0.442 e.$Å^{-3}$	0.884 and -0.888 e.$Å^{-3}$

4. Assignment of ^{1}H NMR peaks of 1

Five groups of ^{1}H NMR aliphatic peaks were observed in the ^{1}H NMR spectrum of **1** in CD_3CN (Figure S1), corresponding to five types of aliphatic protons belong to pentaethylene glycol moiety. It's necessary to unambiguously assign the ^{1}H NMR peaks to ethylene protons, because the pentaethylene glycol moiety is crucial in cation binding.

First of all, the singlet peak at δ = 3.52 ppm (Figure S1) could be easily assigned to proton ***e***. Triplet peak at δ = 4.48 ppm (Figure S1) was assigned to proton ***a*** because of the cross peak between proton ***a*** and one triazine carbon (Figure S2, star marked carbon) observed in HMBC spectra (Figure S3). Moreover, HMBC spectra helped to assign peak at δ = 68.17 ppm to carbon ***b*** by the observation of cross peak between proton ***a*** and carbon ***b*** (Figure S4), and multiplet peak at δ = 3.56 ppm to proton ***c*** by observation of cross peak between carbon ***b*** and proton ***c*** (Figure S4). HSQC then assigned the triplet peak at δ = 4.48 ppm to proton ***b*** that directly linked with carbon ***b*** (Figure S5). Finally, last multiplet peak at δ = 3.55 ppm was assigned to proton ***d***. The farther protons locate away from triazine moiety, the higher field NMR signals are, which reflects the electron-deficient nature of triazine moiety.

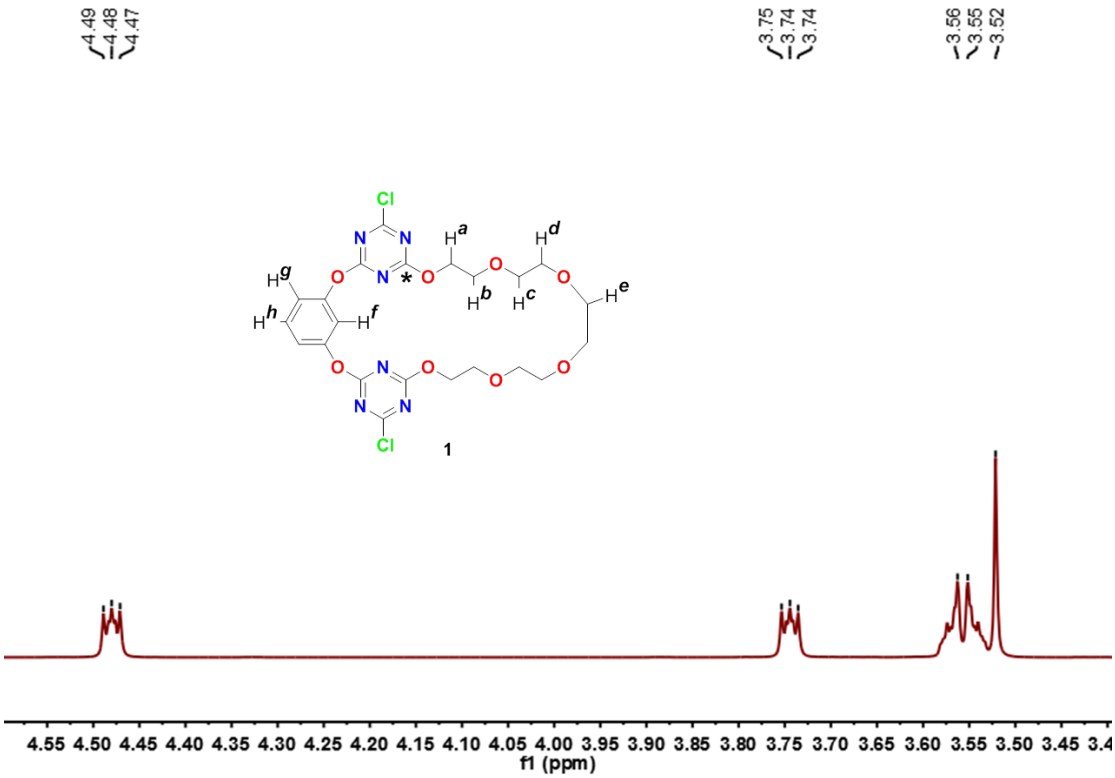

Figure S2. Partial ^{1}H NMR spectra of **1** in CD_3CN (298 K).

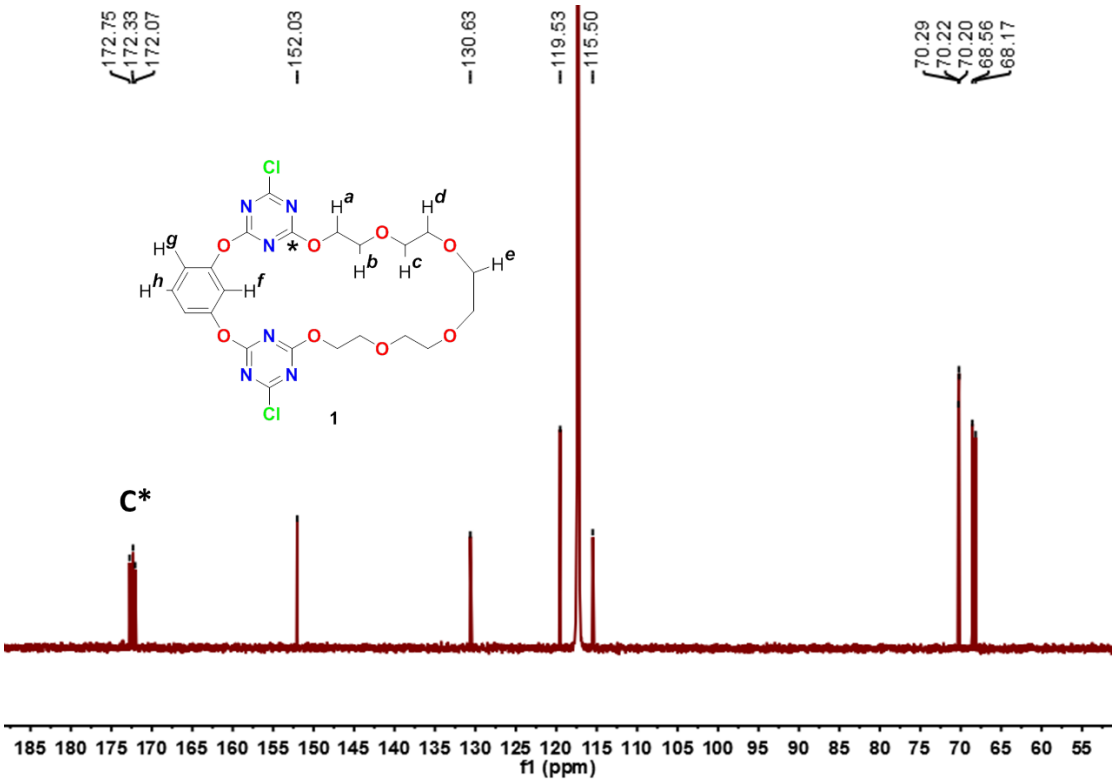

Figure S3. ^{13}C NMR spectra of **1** in CD_3CN (298 K).

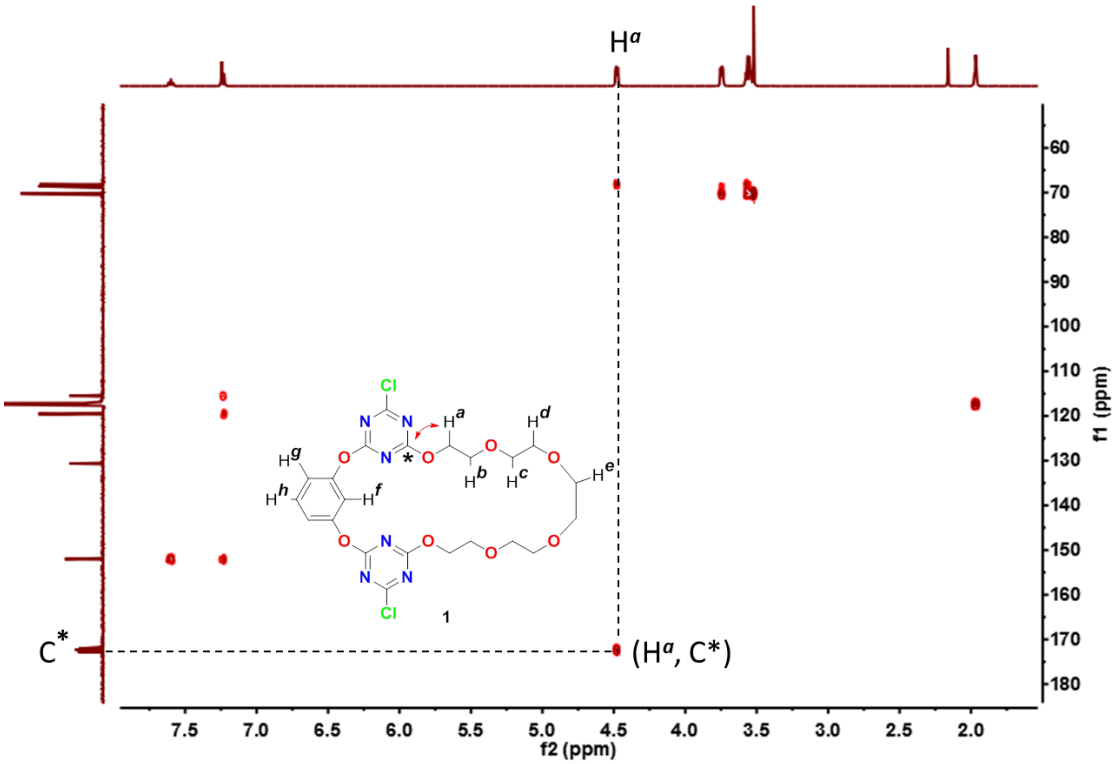

Figure S4. HMBC spectra of **1** in CD_3CN (298 K). Cross peak between proton ***a*** and triazine carbon was showed.

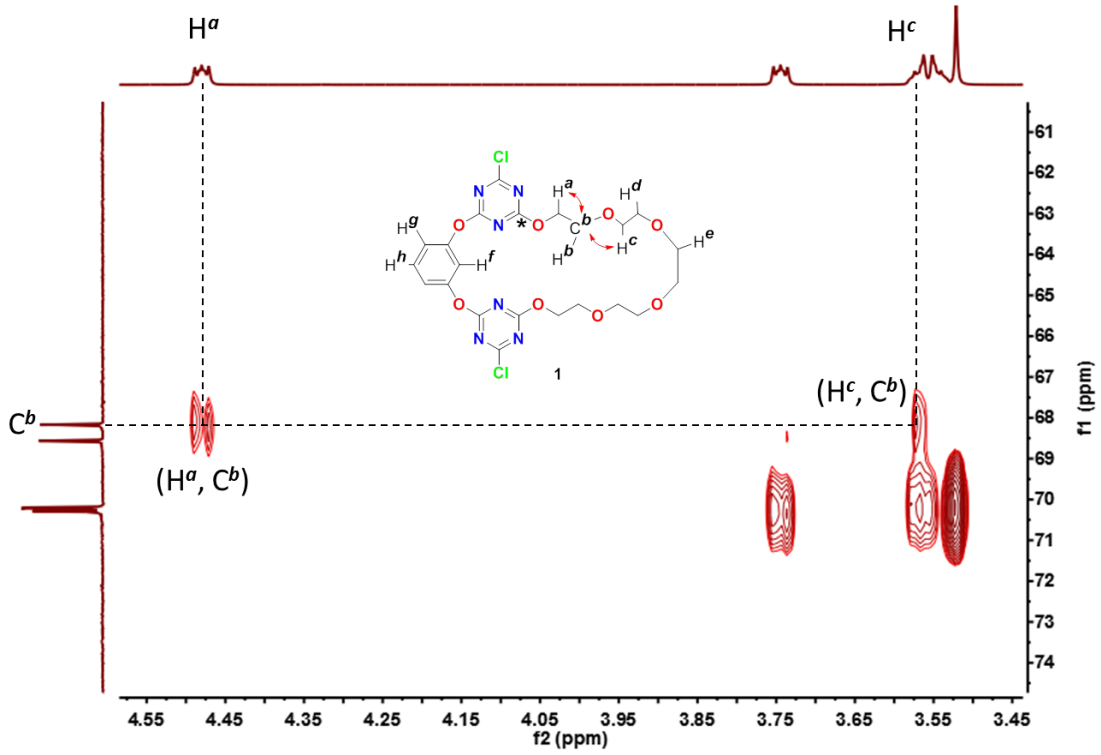

Figure S5. Partial HMBC spectra of **1** in CD_3CN (298 K). Cross peaks between proton ***a*** and carbon ***b***, carbon ***b*** and proton ***c*** were showed.

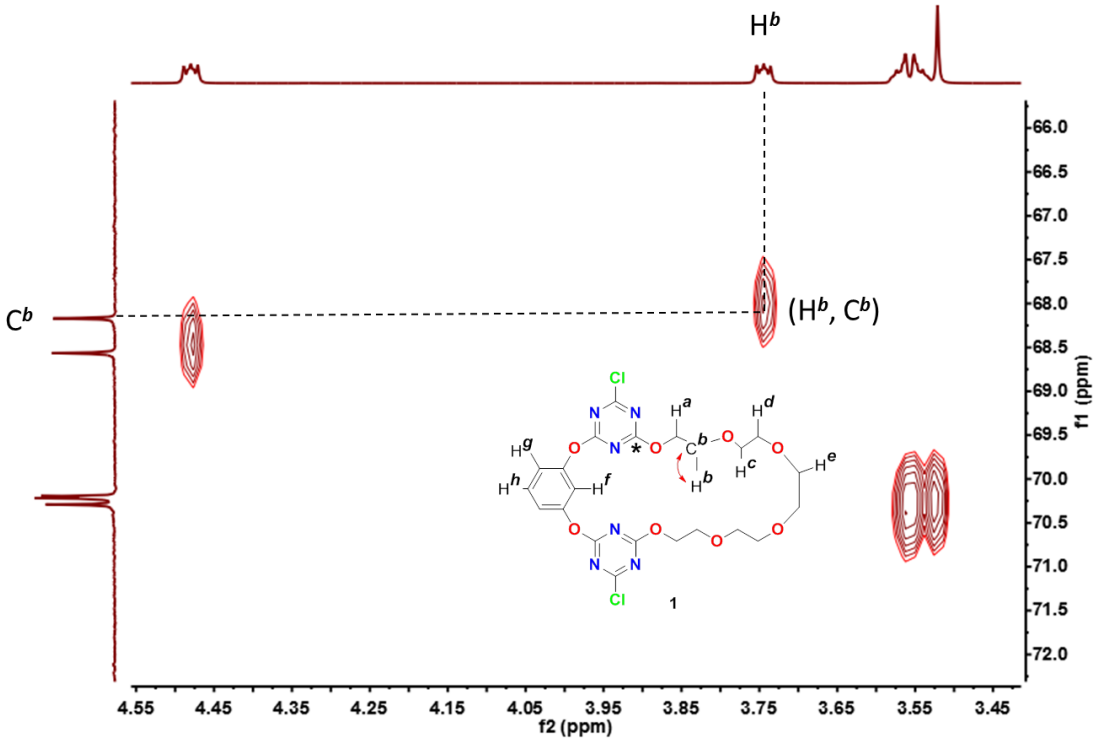

Figure S6. Partial HSQC spectra of **1** in CD_3CN (298 K). Cross peak between proton ***b*** and directly linked carbon ***b*** was showed.

5. ^{1}H NMR spectra of 1 with anions

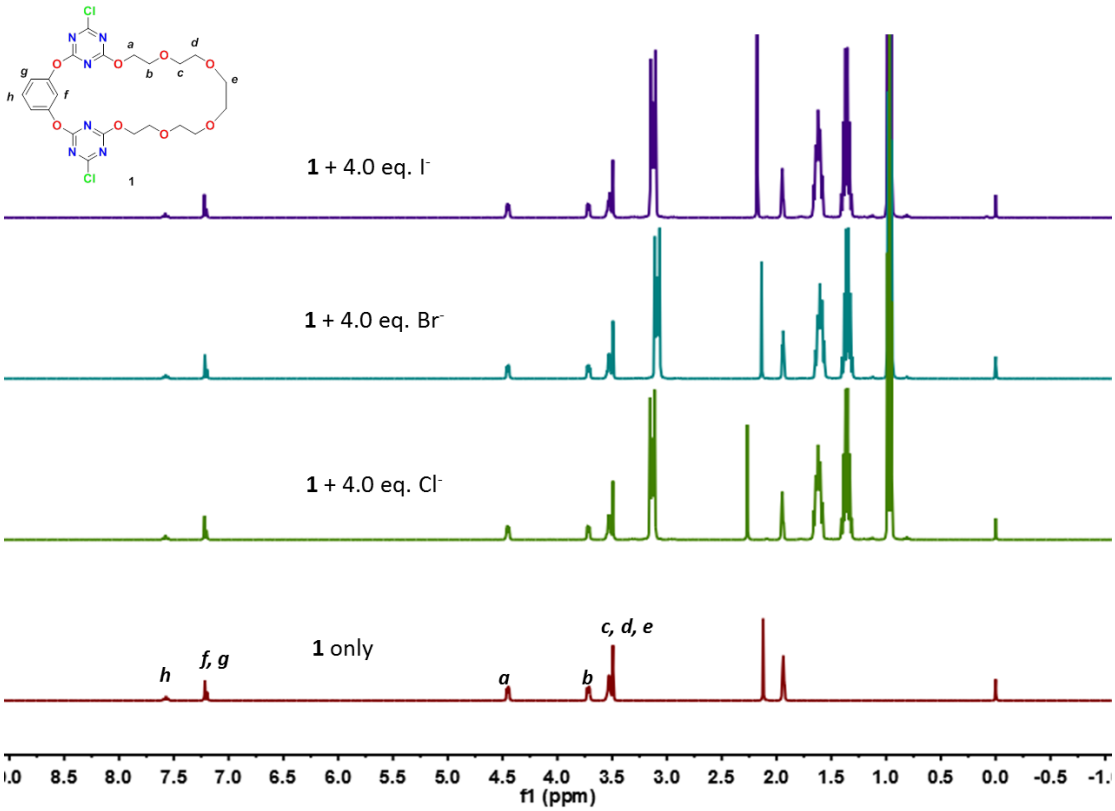

Figure S7. ^{1}H NMR Spectra (CD_3CN) of **1**, **1** + 4.0 eq. NBu_4Cl, **1** + 4.0 eq. NBu_4Br, and **1** + 4.0 eq. NBu_4I, from bottom to top.

6. ^{1}H NMR titration and data analysis for binding of 1 with cations

Titration method

A host stock solution contains 1.05×10^{-2} M **1** in deuterated acetonitrile was prepared. 500 uL host stock solution was added in an NMR tube sealed with a rubber septum. An initial spectrum was recorded and additional spectra were obtained after aliquots of salt ($LiClO_4$, $NaClO_4$, KPF_6, $Mg(ClO_4)_2$, $Ca(ClO_4)_2\cdot4H_2O$) solution (salts solutions were prepared by using forementioned host stock solution as solvent to avoid dilution) was injected sequentially using a microsyringe.

Data analysis

The ethylene proton ***a***, ***b***, ***e*** are the most sensitive protons towards cation binding. For this reason, the chemical shift changes of proton ***a***, ***b***, ***e*** were used to fit the cation binding. Binding of Li^+, Na^+ were found to be too weak to induced significant chemical shift changes. Binding constants were fitted by ***HypNMR 2004***[S1] using a 1:1 binding stoichiometry.

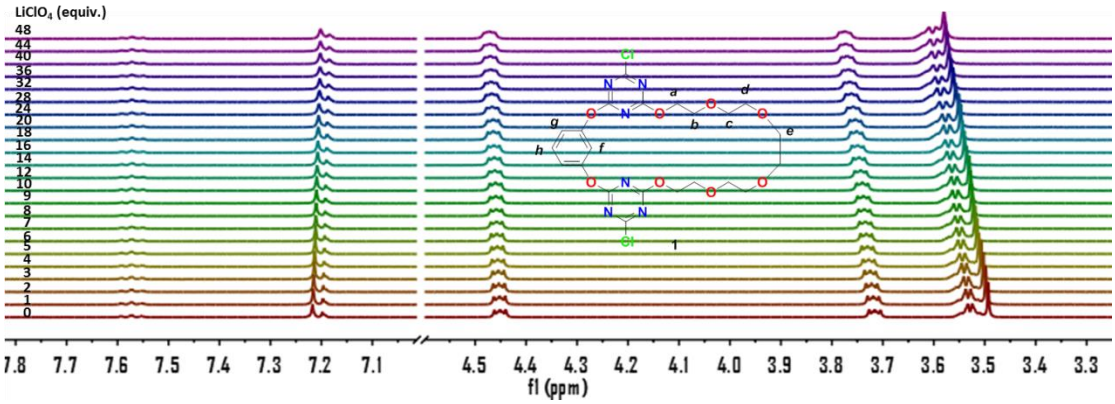

Figure S8. ^{1}H NMR titration of **1** (1.00×10^{-2} M, CD_3CN) with increasing equivalents of $LiClO_4$ added.

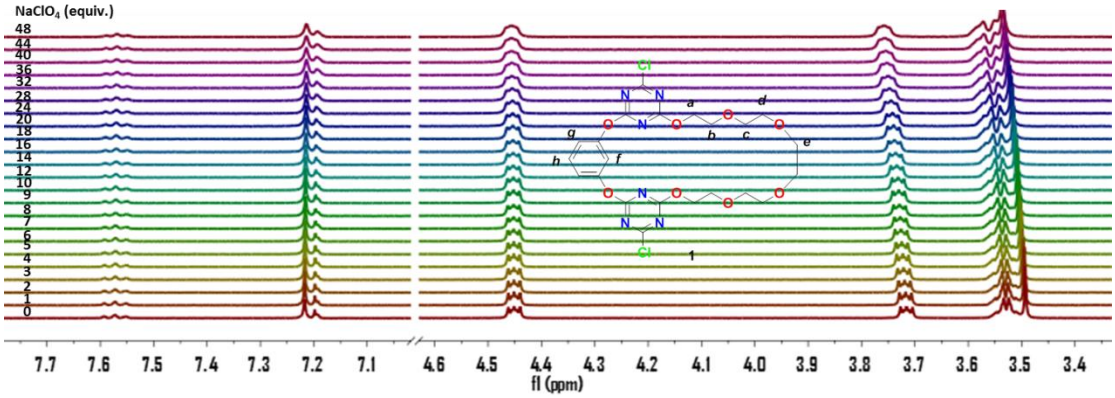

Figure S9. ^{1}H NMR titration of **1** (1.00×10^{-2} M, CD_3CN) with increasing equivalents of $NaClO_4$ added.

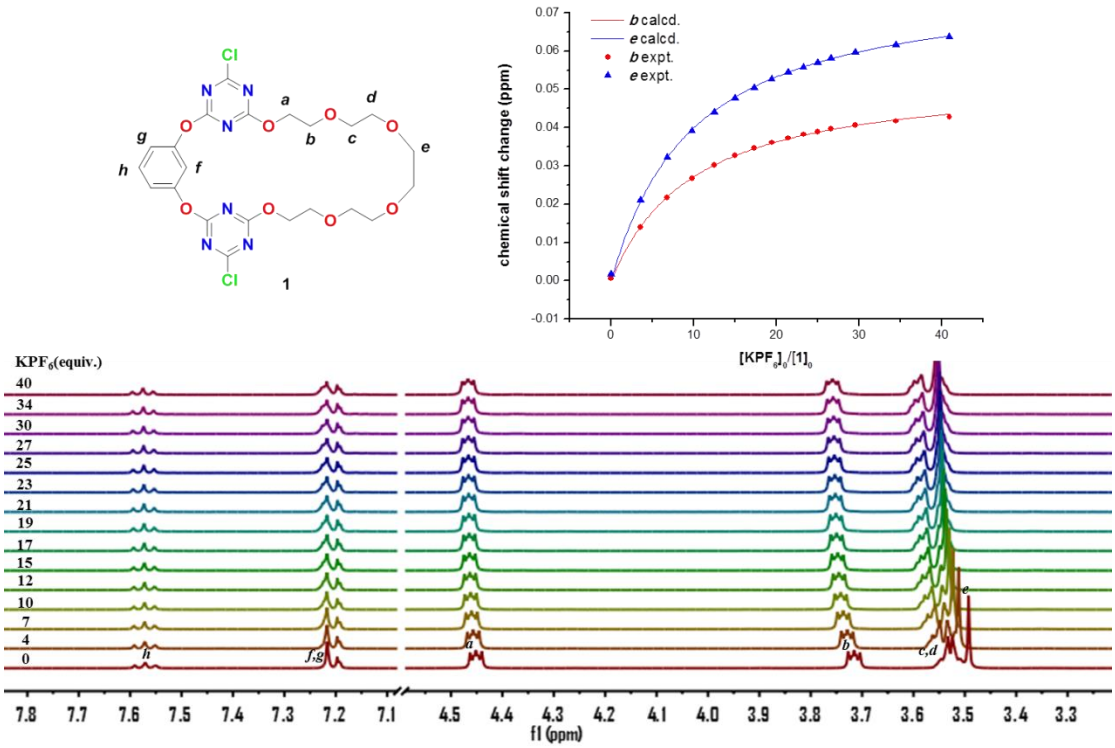

Figure S10. ^{1}H NMR titration of **1** (1.05×10^{-2} M, CD_3CN) with increasing equivalents of KPF_6 (stock solution contains 1.05×10^{-2} M **1** to avoid dilution) added.

Table S3. ***HypNMR 2004*** output for **1** binding K^+ based on 1:1 binding stoichiometry

	Value (M^{-1})	Relative Standard Deviation(%)	Sigma
***K*(1 K^+)**	10	3	0.0002

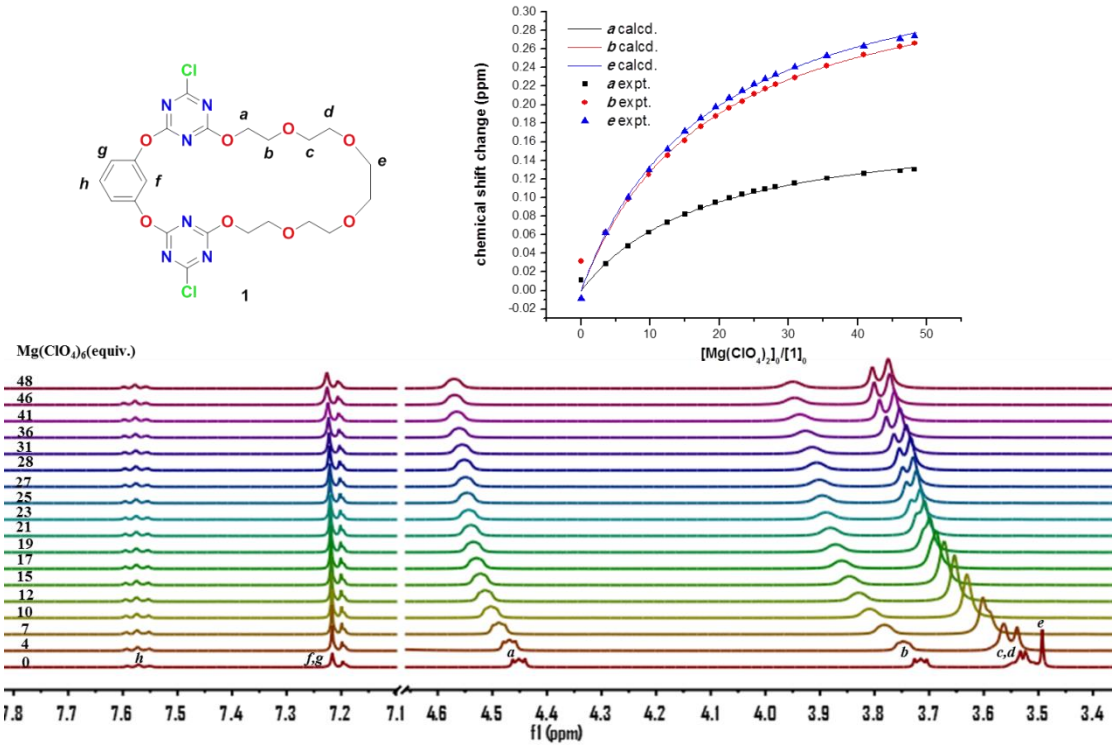

Figure S11. ^{1}H NMR titration of **1** (1.05×10^{-2} M, CD_3CN) with increasing equivalents of $Mg(ClO_4)_2$ (stock solution contains 1.05×10^{-2} M **1** to avoid dilution) added.

Table S4. ***HypNMR 2004*** output for **1** binding Mg^{2+} based on 1:1 binding stoichiometry

	Value (M^{-1})	Relative Standard Deviation(%)	Sigma
$K(\mathbf{1}\cdot Mg^{2+})$	5	3	0.0016

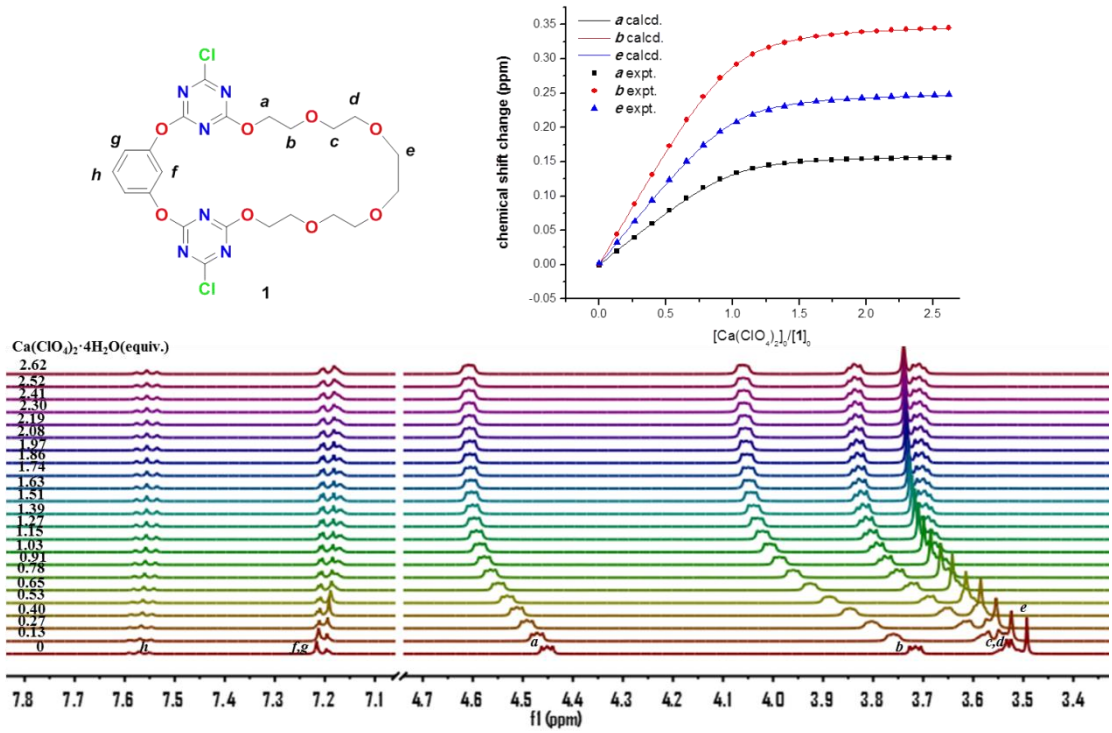

Figure S12. ^{1}H NMR titration of **1** (1.05×10^{-2} M, CD_3CN) with increasing equivalents of $Ca(ClO_4)_2\cdot4H_2O$ (stock solution contains 1.05×10^{-2} M **1** to avoid dilution) added.

Table S5. ***HypNMR 2004*** output for **1** binding Ca^{2+} based on 1:1 binding stoichiometry

	Value (M^{-1})	Relative Standard Deviation(%)	Sigma
***K*(1** Ca^{2+}**)**	2243	2	0.0009

7. ^{1}H NMR titration and data analysis for binding of [1·Ca^{2+}] with anions

Based on caculation, when 2.0 eq. Ca^{2+} was added into the host stock solution, more than 95% **1** will exist as 1:1 complexed form ([**1** Ca^{2+}], this can be caculated from binding constant and initial concentration). Under this condition, we regard the complexed form to be unity, which means the concentration of **1** Ca^{2+} to be the same as the total concentration of **1**. A titration experiment could be conduct to test the binding of [**1** Ca^{2+}] with anions.

Titration method

A host stock solution contains 1.05×10^{-2} M **1** and 2.10×10^{-2} M $Ca(ClO_4)_2\cdot4H_2O$ in deuterated acetonitrile was prepared. 500 ul host stock solution was added in an NMR tube sealed with a rubber septum. An initial spectrum was recorded and additional spectra were obtained after aliquots of salt (Bu_4NX, $X=Cl^-$, Br^-, I^-) solution (salts solutions were prepared by using host stock solution as solvent to avoid dilution except for Bu_4NCl, because precipitate was formed when Bu_4NCl was added into host stock solution. Bu_4NCl solution was prepared by directly dissolving it in deuterated acetonitrile) was injected sequentially using a microsyringe.

Data analysis

The aromatic proton ***f*** are the most sensitive proton towards anion binding, also chemical shift changes could be detected for proton ***a***, ***b***, ***e***, ***g***, ***h***. To realize better fitting, we think both aromatic protons and ethylene protons should be used. For this reason, the chemical shift changes of proton ***a***, ***b***, ***e*** and ***f***, ***g***, ***h*** (particially selected) were used to fit the anion binding. Binding constants were fitted by ***HypNMR 2004*** using a direct 1:2 binding stoichiometry β_{12} (Scheme S3(B)). Although we have tried a stepwise 1:2 binding stoichiometry (Scheme S3(A)), no reasonable results could be obtained.

(**A**) Stepwise 1:2 Binding Stoichiometry:

$$[\mathbf{1} \cdot Ca^{2+}] + X^- \overset{K_{11}}{\rightleftharpoons} [\mathbf{1} \cdot Ca^{2+} \cdot X^-]$$

$$[\mathbf{1} \cdot Ca^{2+} \cdot X^-] + X^- \overset{K_{12}}{\rightleftharpoons} [\mathbf{1} \cdot Ca^{2+} \cdot 2X^-]$$

(**B**) Direct 1:2 Binding Stoichiometry:

$$[\mathbf{1} \cdot Ca^{2+}] + 2X^- \overset{\beta_{12}}{\rightleftharpoons} [\mathbf{1} \cdot Ca^{2+} \cdot 2X^-]$$

(**C**) Calcium Abstraction:

$$[\mathbf{1} \cdot Ca^{2+}] + 2X^- \overset{K\text{ca}}{\rightleftharpoons} \mathbf{1} + CaX_2\,(s)$$

Scheme S3. Possible equilibrations in the ion-pair binding process.

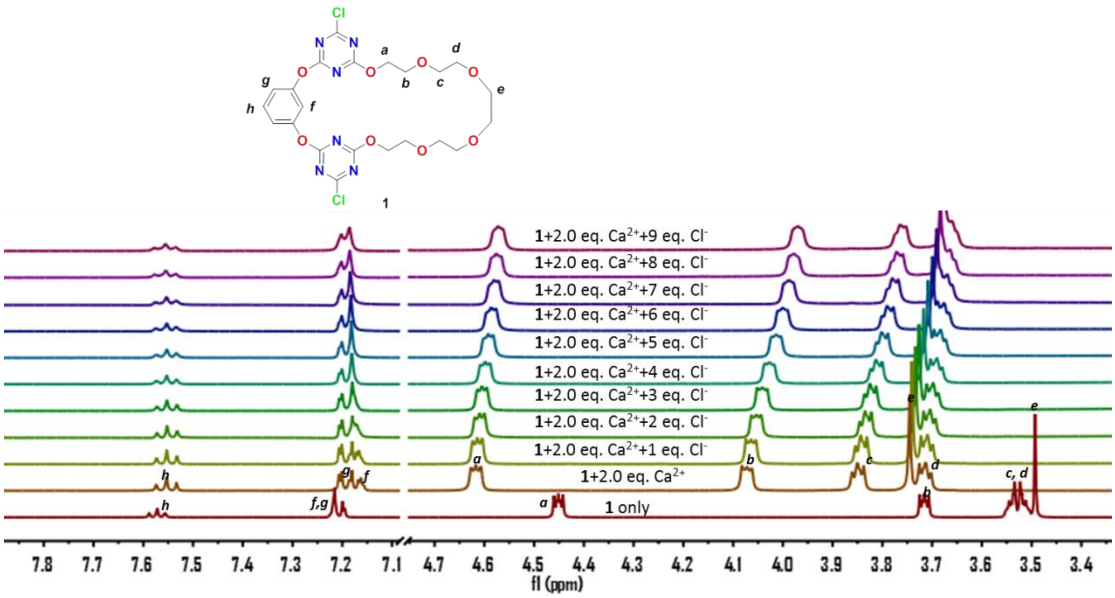

Figure S13. ^{1}H NMR titration in CD_3CN of **1** (1.05×10^{-2} M) and $Ca(ClO_4)_2$ (2.10×10^{-2} M) with increasing equivalents of NBu_4Cl added. Precipitation was observed during addition, also all protons shift towards **1** suggesting chloride abstract calcium from [**1** Ca^{2+}] to form $CaCl_2$ precipitate (Scheme S3 (C)).

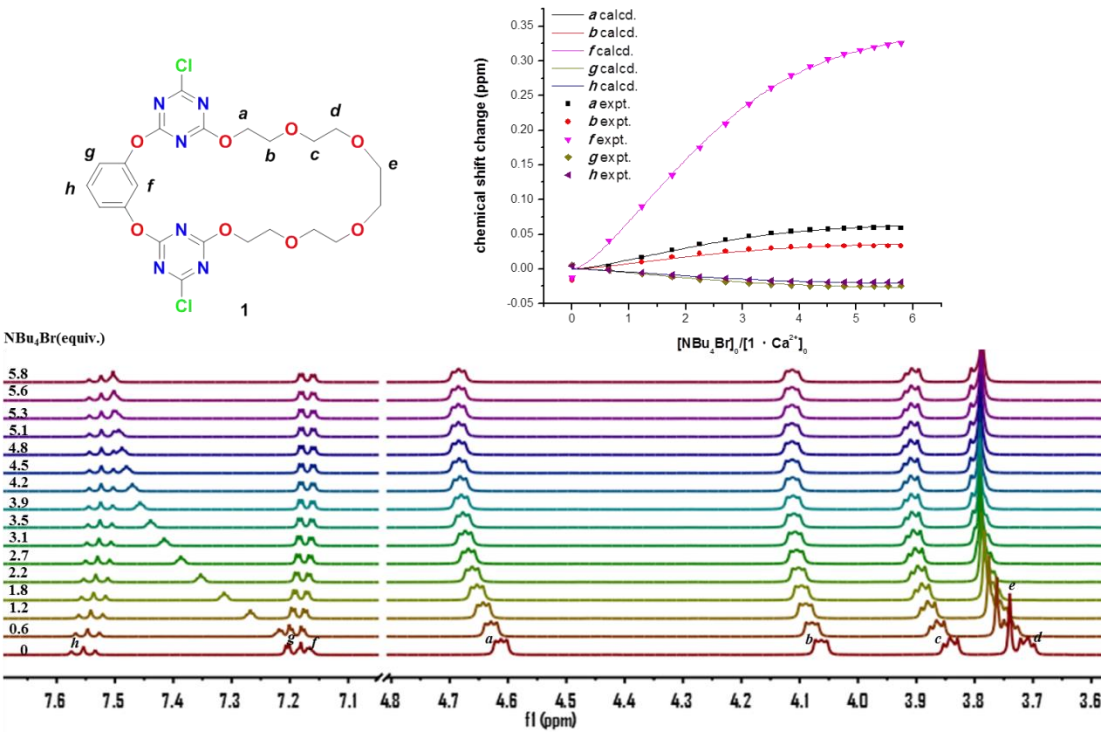

Figure S14. ^{1}H NMR titration in CD_3CN of **1**(1.05×10^{-2} M) and $Ca(ClO_4)_2$ (2.10×10^{-2} M) with increasing equivalents of NBu_4Br (stock solution contains 1.05×10^{-2} M **1** and 2.10×10^{-2} M $Ca(ClO_4)_2$ to avoid dilution) added.

Table S6. ***HypNMR 2004*** output for [**1** Ca^{2+}] binding Br^- based on direct 1:2 binding stoichiometry

	Value (M^{-2})	Relative Standard Deviation(%)	Sigma
β ([**1** Ca^{2+}] $2Br^-$)	5508	5	0.0018

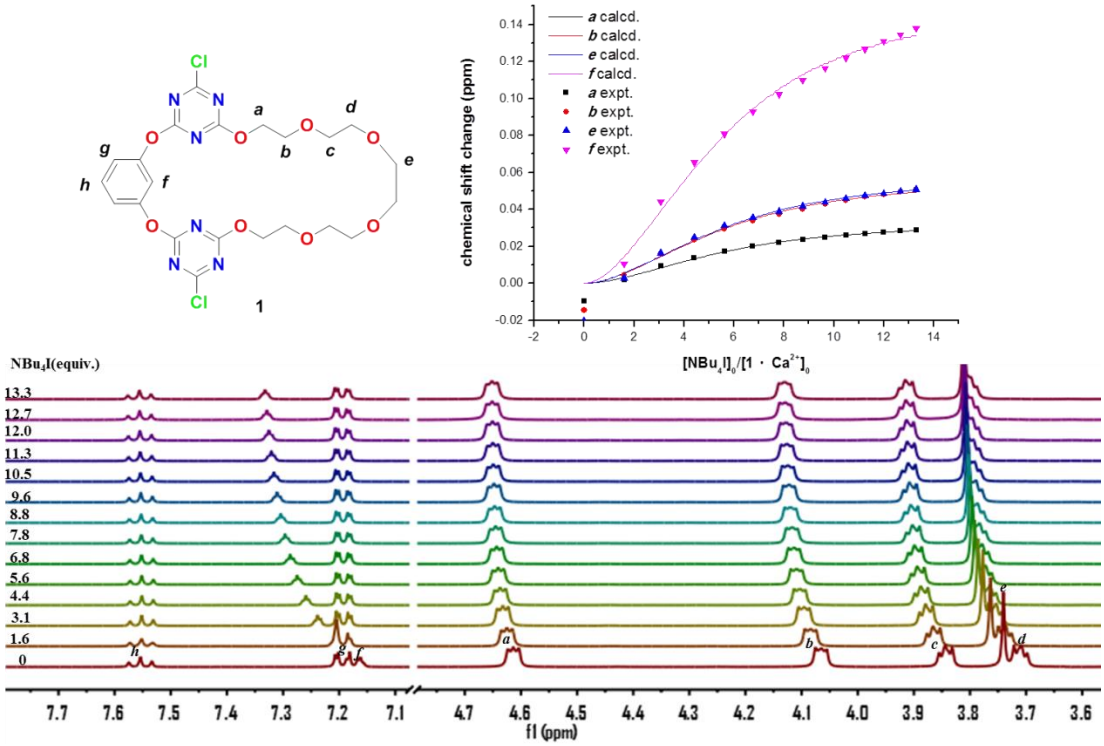

Figure S15. ^{1}H NMR titration in CD_3CN of **1** (1.05×10^{-2} M) and $Ca(ClO_4)_2$ (2.10×10^{-2} M) with increasing equivalents of NBu_4I (stock solution contains 1.05×10^{-2} M **1** and 2.10×10^{-2} M $Ca(ClO_4)_2$ to avoid dilution) added.

Table S7. ***HypNMR 2004*** output for [**1** Ca^{2+}] binding I^- based on direct 1:2 binding stoichiometry

	Value (M^{-2})	Relative Standard Deviation(%)	Sigma
β ([**1** Ca^{2+}] $2I^-$)	477	7	0.0017

8. ^{1}H NMR titration and data analysis for binding of 1 with CaX_2

Titration method

A host stock solution contains 1.05×10^{-2} M **1** in deuterated acetonitrile was prepared. 500 ul host stock solution was added in an NMR tube sealed with a rubber septum. An initial spectrum was recorded and additional spectra were obtained after aliquots of ion pair ($CaBr_2$, CaI_2) solution (solutions were prepared by using host stock solution as solvent to avoid dilution, also to solubilize $CaBr_2$, which can't dissolve well in acetonitrile) was injected sequentially using a microsyringe.

Data analysis

Since the ethylene protons is sensitive to cation binding, and the aromatic protons is sensitive to anion binding, ethylene protons ***a***, ***b***, ***e*** and the aromatic protons ***f***, ***g***, ***h*** were used to fit the ion pair binding. We noticed the chemical shift changes of ethylene protons and aromatic protons keeping the same trends during the adding of $CaBr_2$ and CaI_2 and approximating sauterated when 1 eq. $CaBr_2$ or CaI_2 were added. We think these facts reflect the simultaneous and strong binding of **1** with Ca^{2+}, and Br^- or I^- (CaX_2 ion triplet). For calculation of binding constants, we tried a direct 1:1:2 binding stoichiometry to get the accumulative binding constants ($\beta_{1:1:2}$) (Scheme S4(A)) as generally for positively cooperative systems, it is often quite difficult to accurately determine the stepwise binding constants. We also carried out the stepwise data fitting (Scheme S4(B)) with consideration of intermediate equilibriums and failed to obtain reasonable results.

(**A**) **Direct 1:1:2 Binding Stoichiometry:**

$$\mathbf{1} + Ca^{2+} + 2X^- \overset{\beta_{112}}{\rightleftharpoons} \mathbf{1}\cdot Ca^{2+}\cdot 2X^-$$

(**B**) **Intermediate Equilibriums:**

$$\mathbf{1} + Ca^{2+} \overset{K_1}{\rightleftharpoons} \mathbf{1}\cdot Ca^{2+}$$

$$\mathbf{1} + Ca^{2+} + X^- \overset{\beta_{111}}{\rightleftharpoons} \mathbf{1}\cdot Ca^{2+}\cdot X^-$$

Scheme S4. Direct 1:1:2 binding stoichiometry of **1** binding CaX_2.

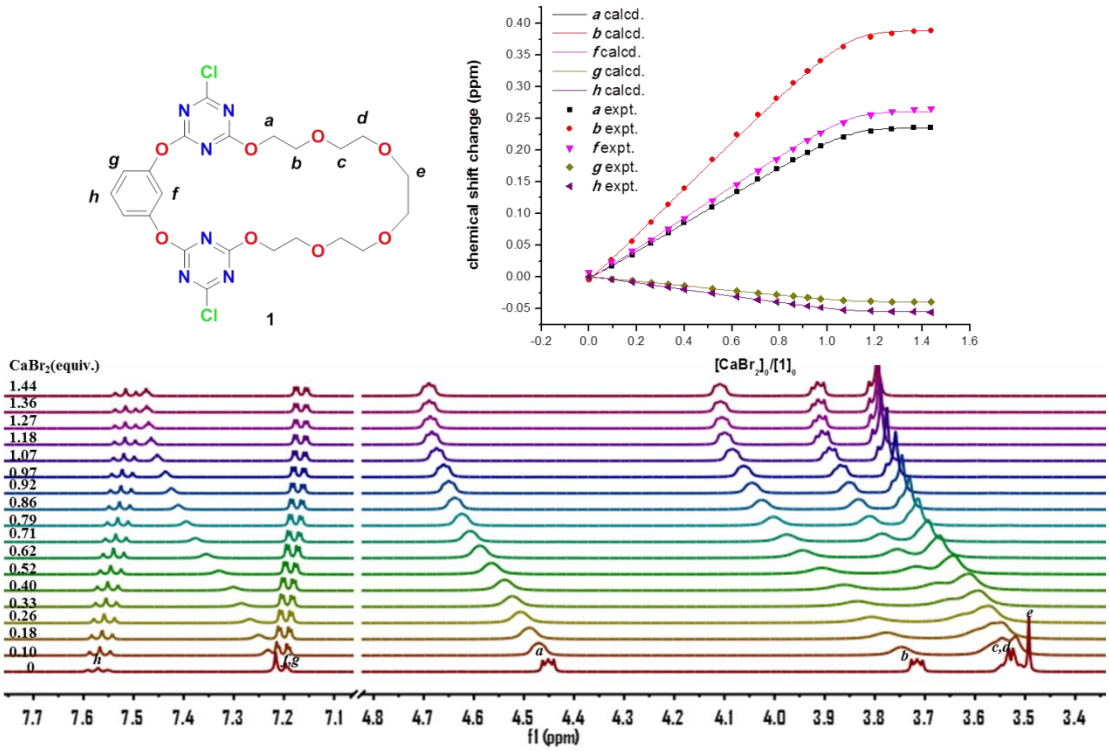

Figure S16. ^{1}H NMR titration in CD_3CN of **1** (1.05×10^{-2} M) and with increasing equivalents of $CaBr_2$ (stock solution contains 1.05×10^{-2} M **1** to avoid dilution) added.

Table S8. ***HypNMR 2004*** output for **1** binding $CaBr_2$ based on direct 1:1:2 binding stoichiometry

	Value (M^{-3})	Relative Standard Deviation(%)	Sigma
β (**1** Ca^{2+} $2Br^{-}$)	1.55×10^{9}	11	0.0017

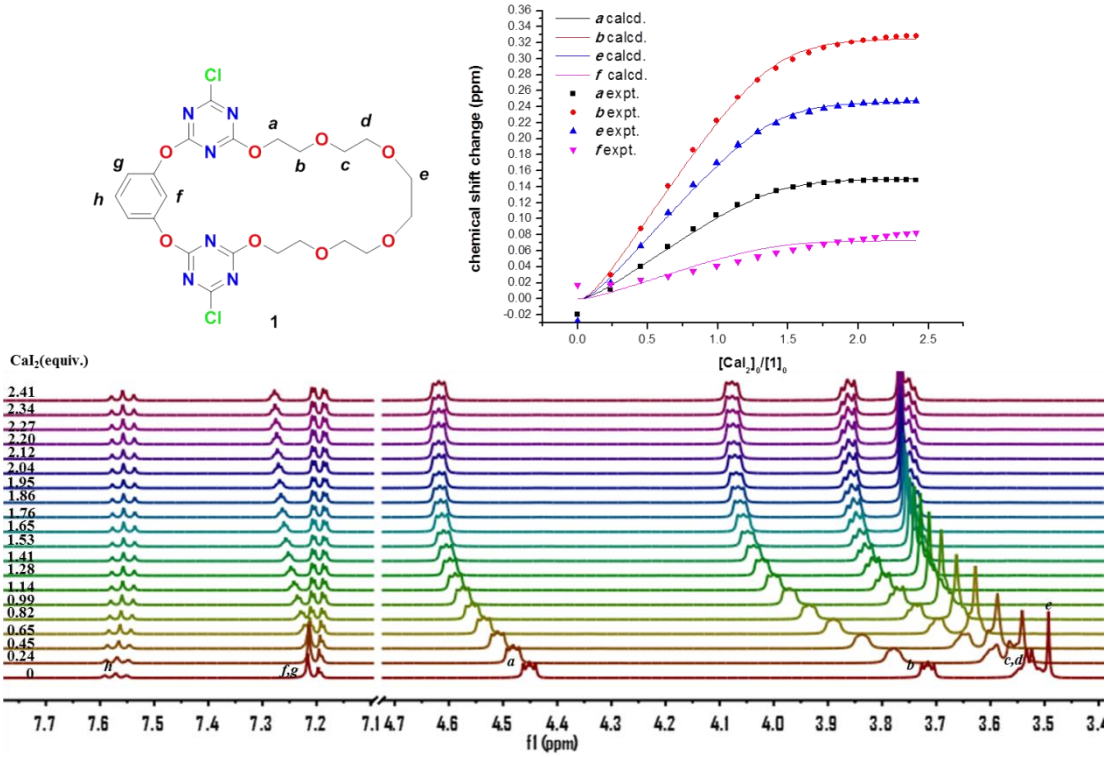

Figure S17. ^{1}H NMR titration in CD_3CN of **1** (1.05×10^{-2} M) and with increasing equivalents of CaI_2 (stock solution contains 1.05×10^{-2} M **1** to avoid dilution) added.

Table S9. ***HypNMR 2004*** output for **1** binding CaI_2 based on direct 1:1:2 binding stoichiometry

	Value (M^{-3})	Relative Standard Deviation(%)	Sigma
β(**1** Ca^{2+} $2I^-$)	1.30×10^{7}	11	0.0043

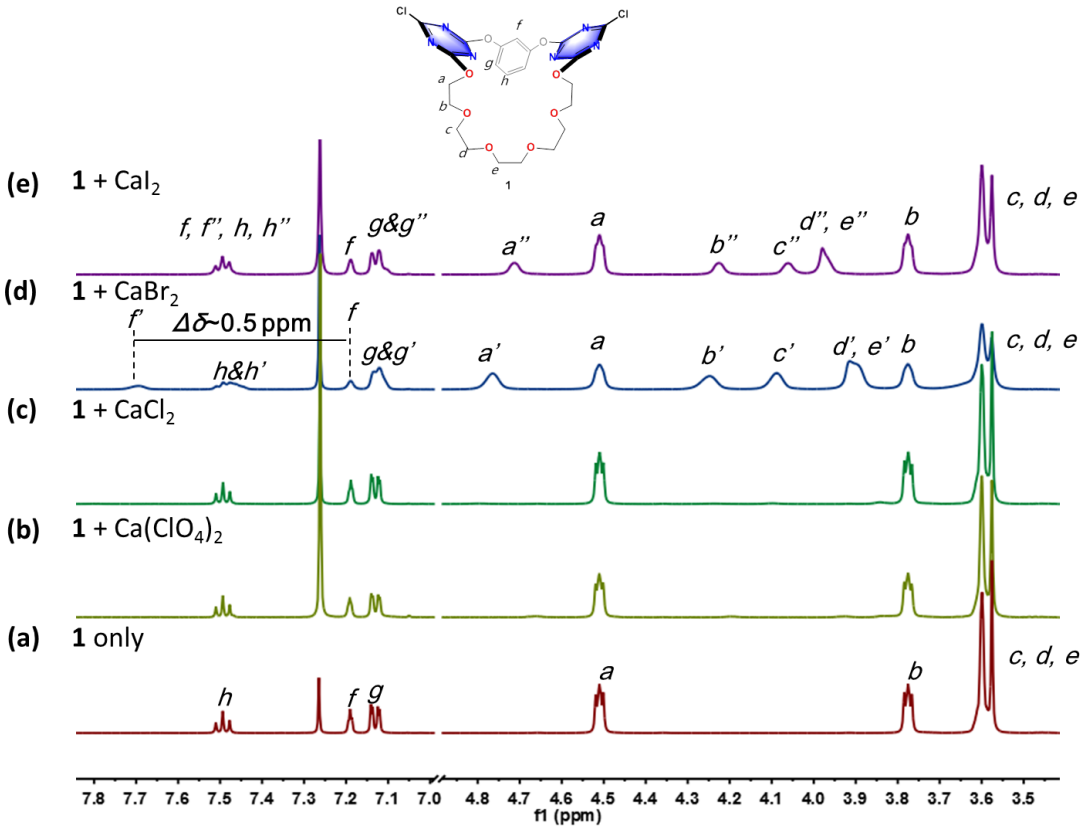

Figure S18. ^{1}H NMR spectra in $CDCl_3$ of **1** (1.05×10^{-2} M) with CaX_2 (5.0 equiv. as solid powder). From bottom to top: (a) **1** only, (b) **1** + $Ca(ClO_4)_2$, (c) **1** + $CaCl_2$, (d) **1** + $CaBr_2$, (e) **1** + CaI_2.

9. ^{1}H NMR titration and data analysis for binding of 2 with $Ca(ClO_4)_2$

Titration Method and **Data Analysis** are similar as those of **1** binding calcium.

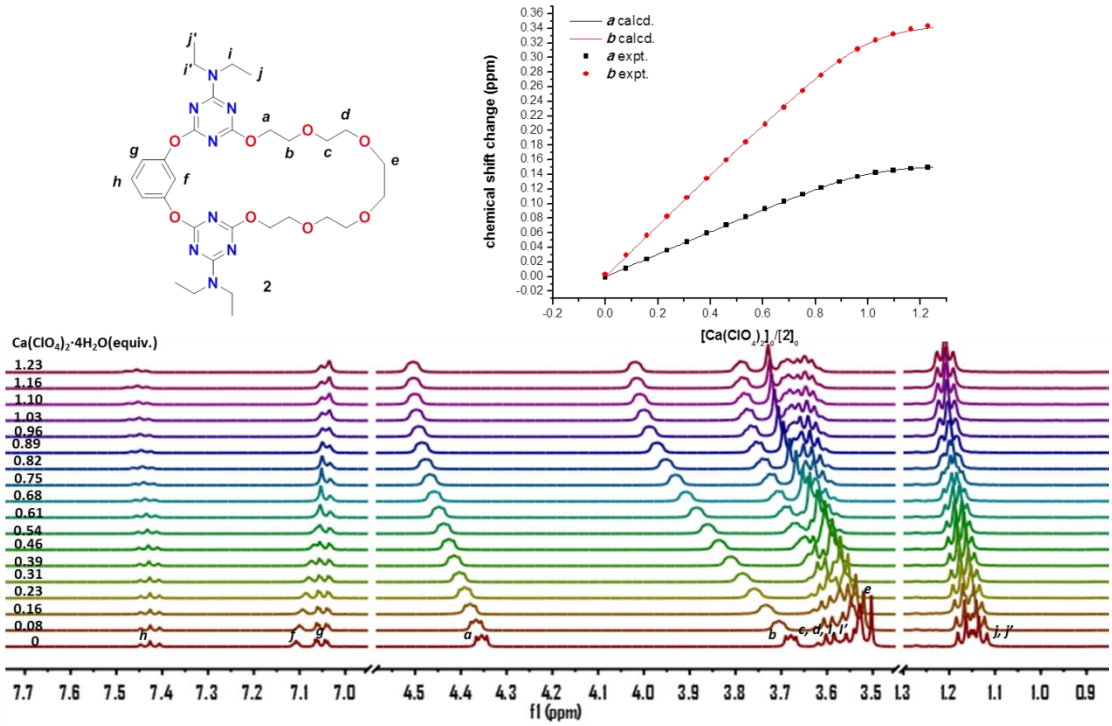

Figure S19. ^{1}H NMR titration of **2**(1.03×10^{-2} M, CD_3CN) with increasing equivalents of $Ca(ClO_4)_2\cdot4H_2O$ (stock solution contains 1.05×10^{-2} M **2** to avoid dilution) added.

Table S10. ***HypNMR 2004*** output for **2** binding Ca^{2+} based on 1:1 binding stoichiometry

	Value (M^{-1})	Relative Standard Deviation(%)	Sigma
K(**2** Ca^{2+})	8877	12	0.0010

10. ^{1}H NMR titrations for binding of [2 Ca^{2+}] with anions, 2 with $CaBr_2$

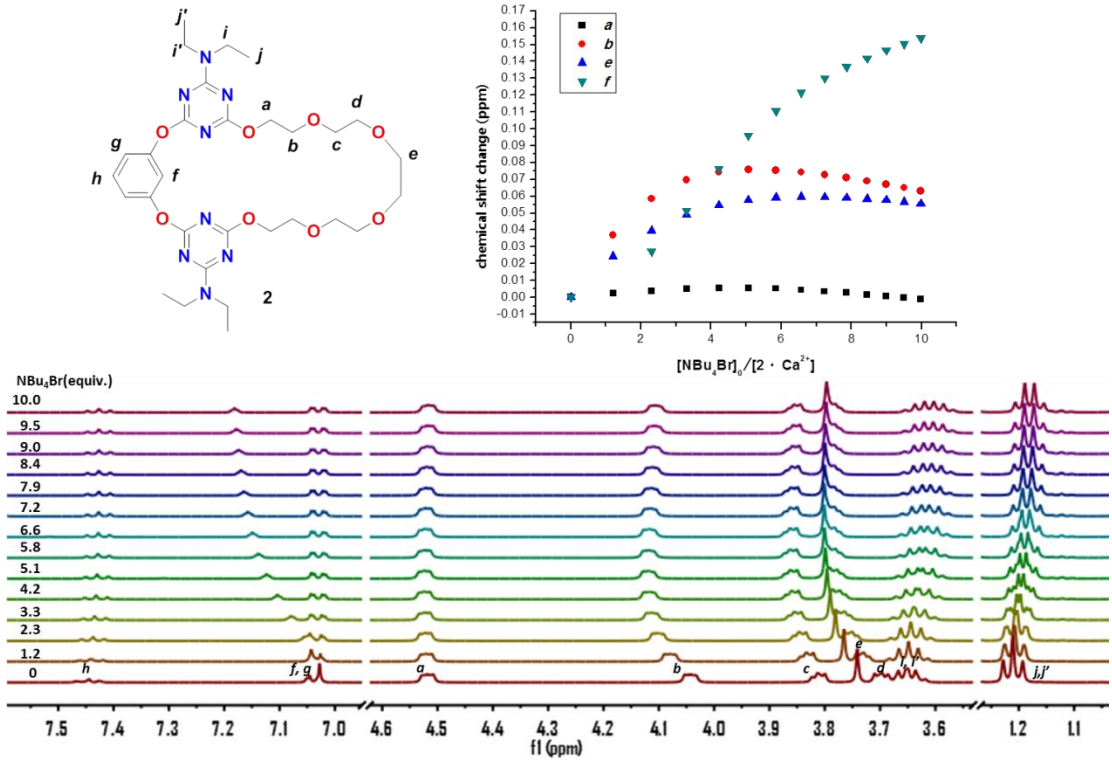

Figure S20. ^{1}H NMR titration in CD_3CN of **2**(1.03×10^{-2} M) and $Ca(ClO_4)_2$ (2.06×10^{-2} M) with increasing equivalents of NBu_4Br (stock solution contains 1.03×10^{-2} M **2** and 2.06×10^{-2} M $Ca(ClO_4)_2$ to avoid dilution) added.

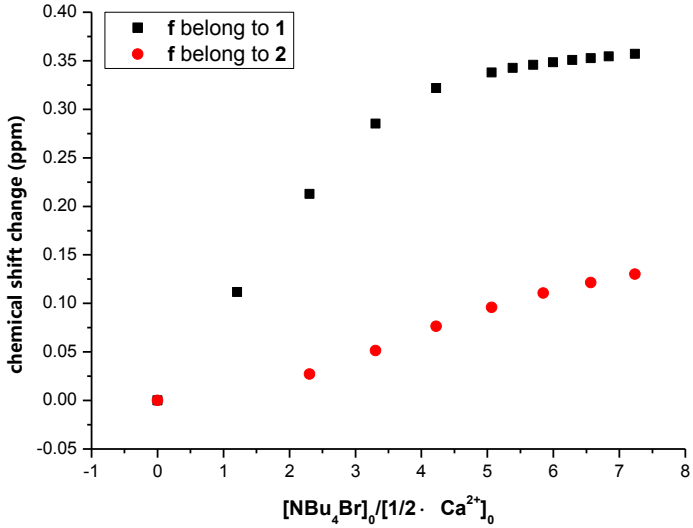

Figure S21. Chemical shift changes for proton *f* belong to **1** (black square) and **2** (red circle) upon addition of NBu_4Br. Chemical shift changes for proton *f* belong to **1** is obviously larger than that belongs to **2**, which suggests stronger binding of **1** with bromide than that of **2**.

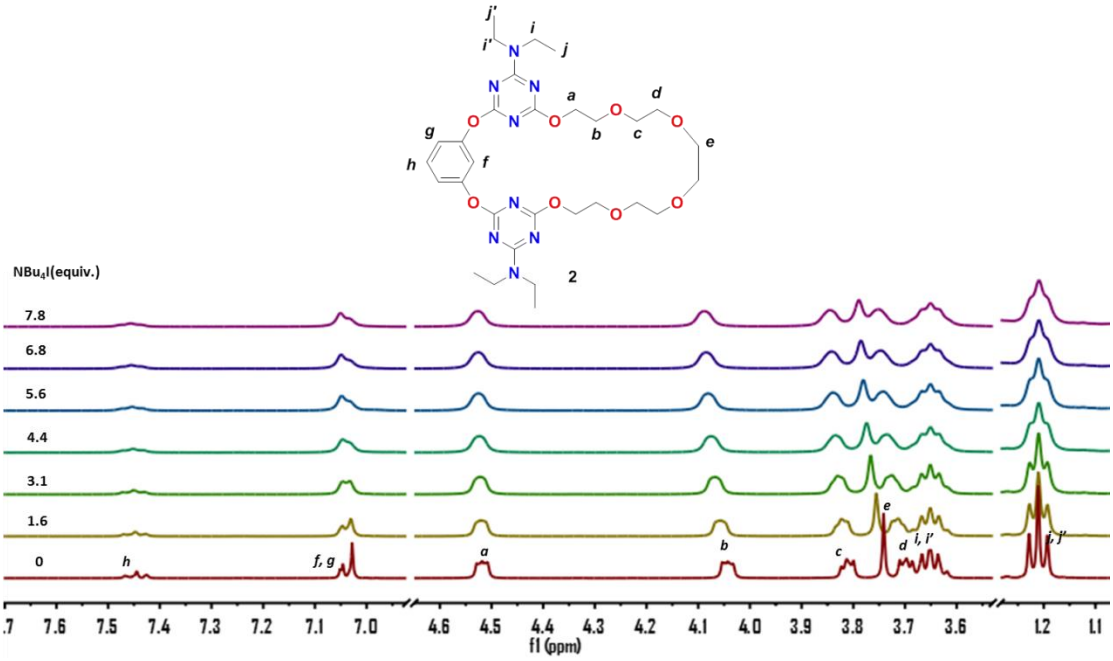

Figure S22. ^{1}H NMR titration in CD_3CN of **2**(1.03×10^{-2} M) and $Ca(ClO_4)_2$ (2.06×10^{-2} M) with increasing equivalents of NBu_4I (stock solution contains 1.03×10^{-2} M **2** and 2.06×10^{-2} M $Ca(ClO_4)_2$ to avoid dilution) added. No significant chemical shift could be observed for all protons, which suggests weak binding of [**2** Ca^{2+}] with iodide.

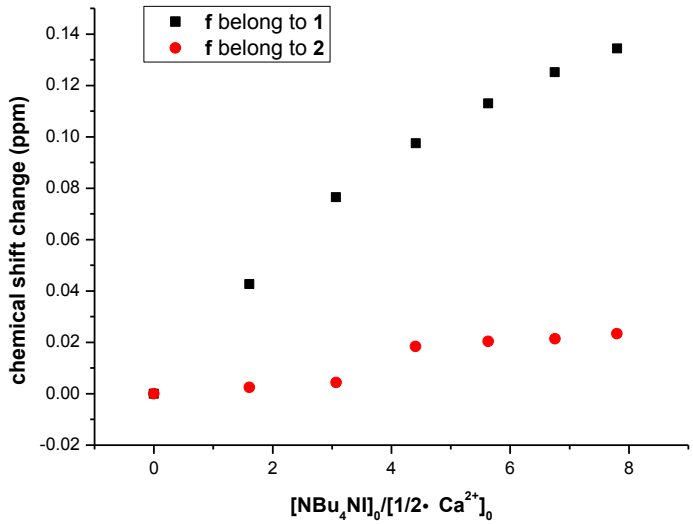

Figure S23. Chemical shift changes for proton *f* belong to **1** (black square) and **2** (red circle) upon addition of NBu_4I. Chemical shift changes for proton *f* belong to **1** is obviously larger than that belongs to **2**, which suggests stronger binding of **1** with iodide than that of **2**.

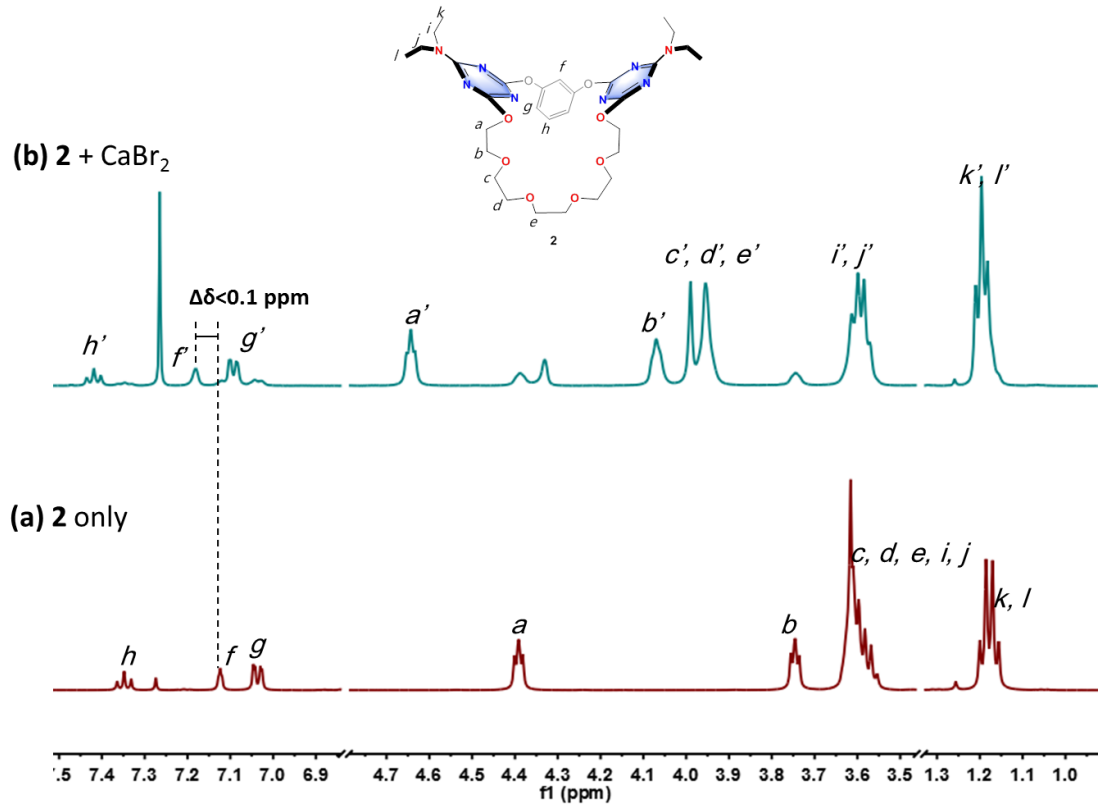

Figure S24. ^{1}H NMR spectra in $CDCl_3$ of (a) **2** (1.05×10^{-2} M M) and (b) **2** + $CaBr_2$ (5.0 eq. as solid powder).

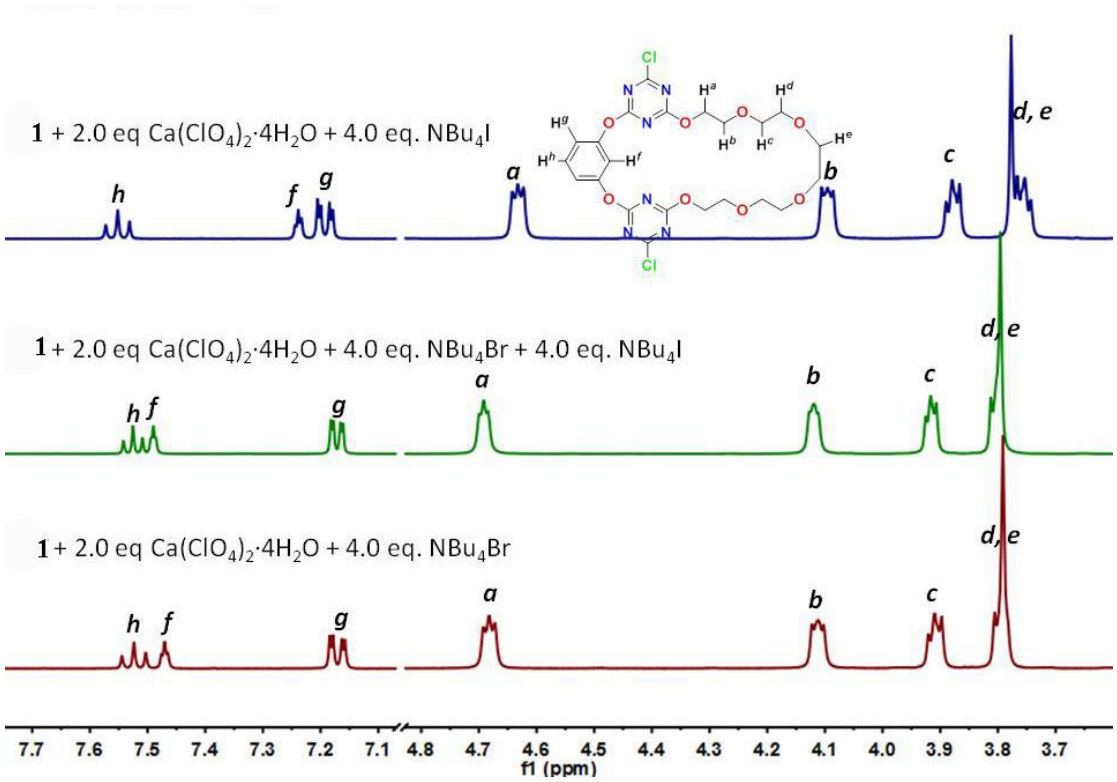

Figure S25. Selective binding of **1** to $CaBr_2$ in the presence of CaI_2.

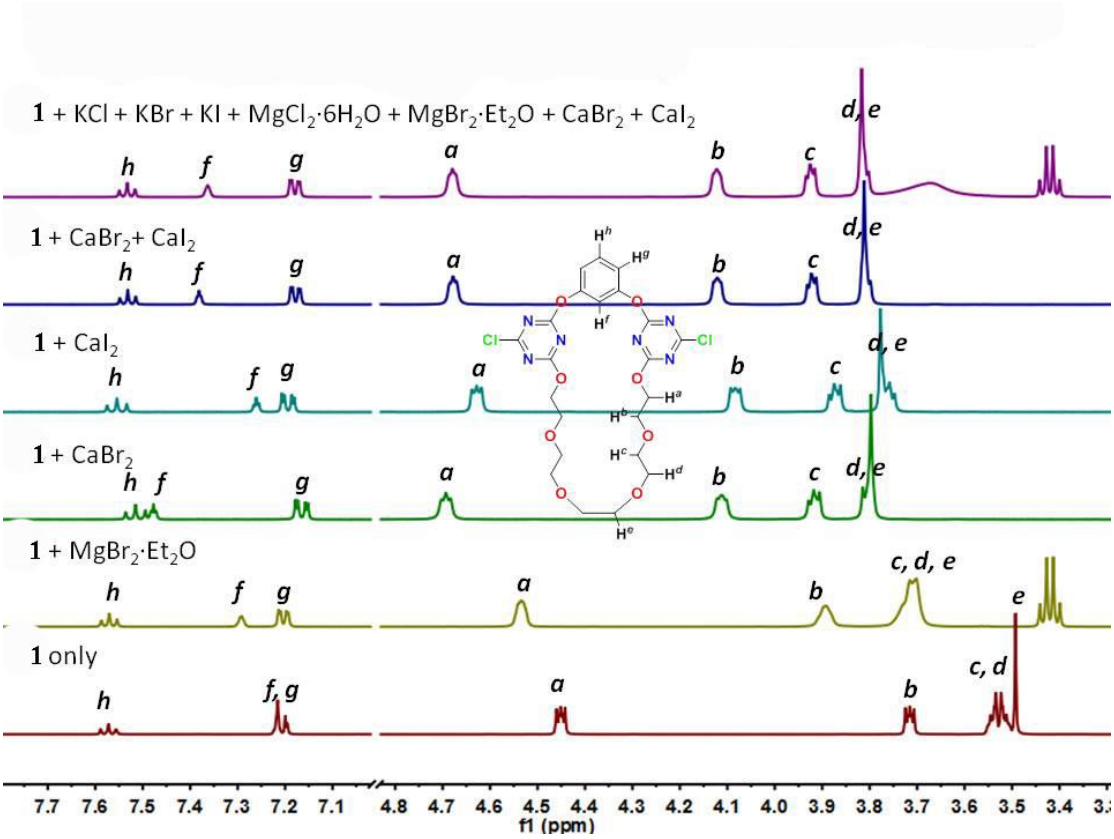

Figure 26. Selective solubilization of CaX_2 in the presence of other salts.

11. ESI-MS of 1 with $CaBr_2$ and CaI_2

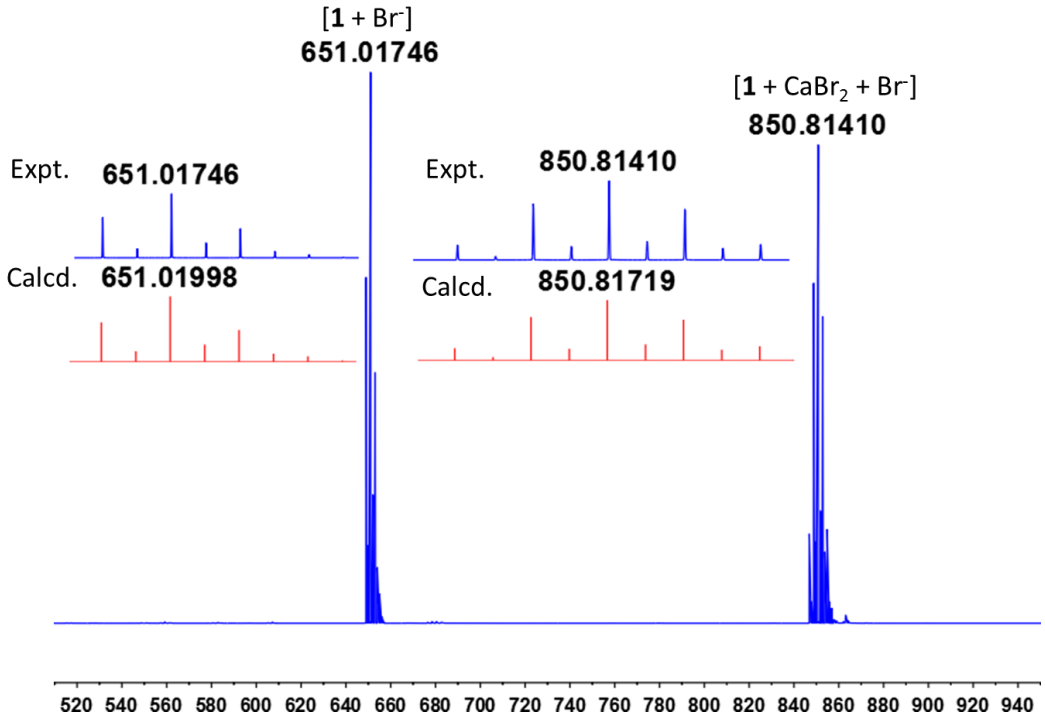

Figure S27. ESI-MS spectra (negative mode) of **1** and $CaBr_2$ (top). Insert is the comparison of experimental and calculated results.

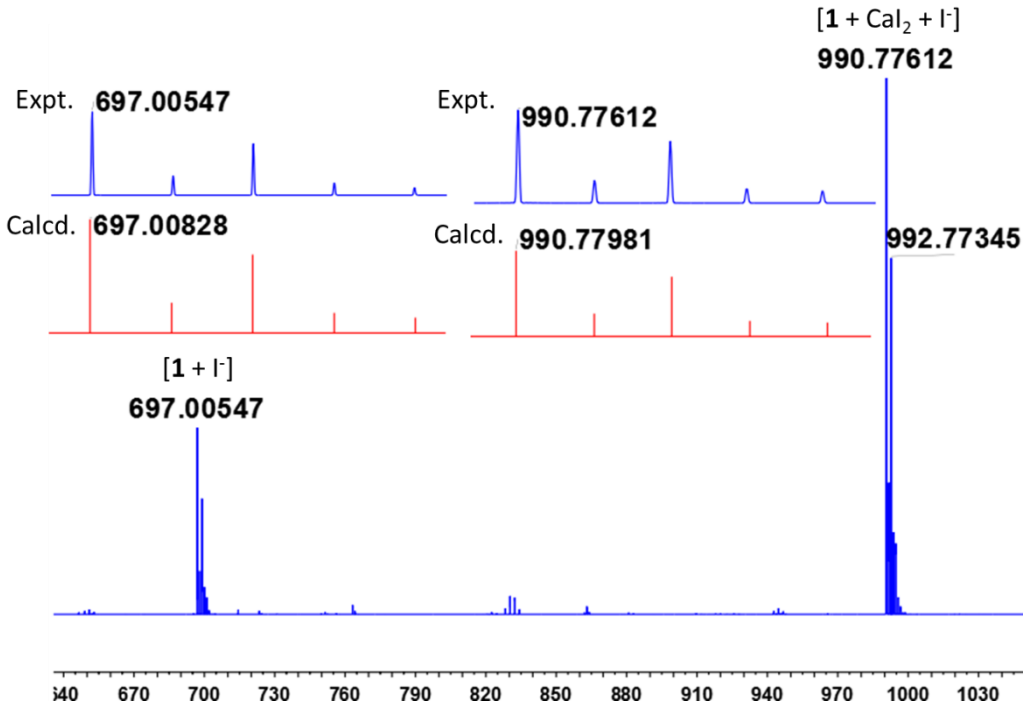

Figure S28. ESI-MS spectra (negative mode) of **1** and CaI_2 (top). Insert is the comparison of experimental and calculated results.

12. Solution Structure of CaX_2 + 1 complexes from dielectric relaxation spectroscopy

Experimental Methods

Dielectric spectra were recorded for solutions of CaI_2, equimolar solutions of CaI_2+**1**, and equimolar solutions of $CaBr_2$+**1** in acetonitrile (Merck, HPLC Plus, >99.9%). ~1g of samples of CaI_2 (c_{salt}= 10, and 20 mM), equimolar CaI_2+**1** (39 mM of **1,** 39 mM CaI_2), and equimolar $CaBr_2$+**1** (50 mM of **1,** 50 mM $CaBr_2$) were prepared gravimetrically on an analytical balance. Both salts were purchased as anhydrous salts from Alfa Aesar and used without further purification. Dielectric spectra as a function of concentration were obtained by gravimetrically adding the appropriate amount of acetonitrile to dilute the samples. Thus, spectra at c_{salt}= 10, 20, 30, and 39 mM for CaI_2+**1**, and at c_{salt}= 10, 20, 30, 40, and 50 mM $CaBr_2$+**1** were measured. Dielectric spectra were recorded with a frequency domain reflectometer based on an Anritsu Vector Star MS4647A vector network analyzer (VNA) together with an open-ended coaxial probe based on 1.85mm coaxial connectors at frequencies, ν, ranging from 0.1 to 10 GHz.[S2]

Ab initio calculations

To compare the DRS results to the crystallography results, we have calculated the electronic structure of [**1** CaI_2] and [**1** $CaBr_2$**]** based on their crystal structure (neglecting co-crystalized solvent molecules). Quantum chemical calculations were performed using the ORCA program package[S3] at the HF/def-SVP[S4–6] level of theory within the resolution of identity.[S7,8] Solvation effects due to acetonitrile were taken into account using the COSMO model.[S9] These calculations reveal that the electrical dipole moment, μ, of [**1** CaI_2] is more than three times higher than the dipole moment of [**1** $CaBr_2$**]** (see Figure S29).

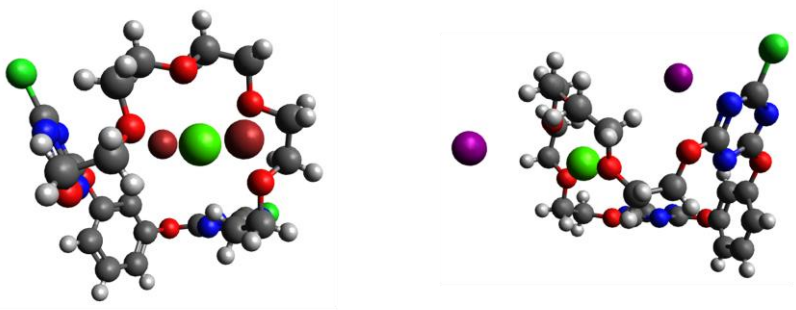

Figure S29. Structures of the [**1** $CaBr_2$**]** complex and [**1** CaI_2] as obtained from crystallography and used for calculating the electrical dipole moment.

DRS results

In an DRS experiment the complex dielectric permittivity of a sample, $\hat{\varepsilon}(\nu) = \varepsilon'(\nu) - i\varepsilon''(\nu)$, is recorded as a function of the field frequency, ν, with ε' being the dielectric permittivity, and ε'' the dielectric loss. For the rotation of dipolar species, a relaxation process with a dispersion in $\varepsilon'(\nu)$ and a peak in the $\varepsilon''(\nu)$ is observed, where the peak frequency scales with the molecular volume of the dipolar species and the viscosity of the solution.[S10] For electrolyte solutions with mobile ions Ohmic loss (conductivity) additionally contributes to $\varepsilon''(\nu)$.

In Figure S30a we show the spectra for solutions of $CaBr_2$+**1**. These spectra are dominated by a dispersion in $\varepsilon'(\nu)$ and a corresponding loss contribution at ν >4 GHz. These features can be attributed to the orientational relaxation of acetonitrile, which is centered at ~ 50 GHz[S11] at room temperature and extends to the frequency range studied here. Upon increasing concentration of $CaBr_2$+**1**, the permittivities are somewhat reduced, which stems from the decreasing volume density of acetonitrile. There are however no indications for the emergence of a dipolar relaxation due to [**1** $CaBr_2$**]**.

In contrast to the nearly exclusive contribution of the solvent to the spectra for solutions of $CaBr_2$+**1**, for solutions of CaI_2 in acetonitrile (CaI_2 is somewhat soluble in acetonitrile) a weak relaxation is observed at ~ 300 MHz, which increases in amplitude with increasing concentration of the salt (Fig. S30b). Such low frequency relaxation can be assigned to rotational relaxation of dipolar ion-pairs in solution[S12]

and can also be observed for solutions of CaI_2+**1** (Fig. 30c).

To quantify the contribution of both relaxations to the spectra, we fit a relaxation model based on two Debye-type relaxations to the spectra:

$$\hat{\varepsilon}(\nu) = \frac{S_1}{1+(i2\pi\nu\tau_1)} + \frac{S_2}{1+i2\pi\nu\tau_2} + \varepsilon_\infty + \frac{\kappa}{i2\pi\nu\varepsilon_0} \qquad \text{(S1)}$$

where S_1 and τ_1 are the relaxation strength and relaxation time of the ion-pair relaxation, respectively. S_2 and τ_2 account for the orientational relaxation of acetonitrile. The last term of eq S1 accounts for the Ohmic loss contribution with κ being the dc conductivity. ε_0 is the permittivity of free space and ε_∞ (which was fixed to 3.33)[S11] is the high frequency limiting permittivity. For solutions of $CaBr_2$+**1** the lower frequency relaxation (first term of eq S1) was omitted.

As can be seen from Fig. 30, such fits describe the experimental spectra with values for the lower frequency relaxation times of $\tau_1 \approx 500$ ps and for the acetonitrile relaxation of $\tau_2 \approx 4$ ps very well. Note, that to reduce the number of adjustable parameters we set $\tau_1 = 500$ ps for solutions with low solute concentration (10 and 20 mM CaI_2+**1**; 10mM CaI_2). The contribution of the lower frequency relaxation to the dielectric loss as obtained from such fits is shown in Fig. S30d. The thus obtained values for the relaxation amplitudes S_1 and S_2 are shown in Fig. S30e and the obtained conductivities are displayed in Fig. S30f.

From these results we find no evidence for any dipolar relaxation of $CaBr_2$+**1** complexes in solution. Taking the experimental uncertainty into account we estimate the relaxation of such complexes to be $S_1 < 0.3$. As the relaxation strengths scales with the squared electrical dipole moment via Cavell's equation[S13] we thus estimate the electrical dipole moment of $CaBr_2$+**1** complexes to be μ < 8 D, consistent with the calculated dipole moment from the crystal structure (Fig. S29). Hence, the DRS results are consistent with nearly stoichiometric formation of $CaBr_2$+**1**, as found from crystallography (Fig. 4 in the main manuscript) also in solution. This notion is further supported by the negligible dc conductivity of these solutions (Fig. S30f), which shows that there are very few free ions (dissociated from the complexes) present in solution.

As can be seen from the finite values for S_1 (Fig. S30e) and the relatively high conductivity (Fig. S30f), both ion-pairs and free ions can be detected for solutions of CaI_2. For solutions of CaI_2 + **1** both the ion-pair relaxation S_1 (proportional to the concentration of dipolar ion-pairs) and the conductivity (number of free ions) is reduced as compared to solutions of CaI_2 at the same concentration (Figure S30e-f). This can be explained by the binding of CaI_2 ion-pairs and free ions by the receptor molecule. The amplitude of the detected ion-pair relaxation increases with increasing concentrations of CaI_2 + **1**, with $S_1 = 1.6$ at the highest concentration (39 mM). This again is consistent with the formation of dipolar CaI_2 + **1** complexes with $\mu \approx 21$ D (see Cavell's equation[S13]), which is in line with our calculations (Fig. S29). Remarkably, when comparing the values of S_1 with and without **1** at the same concentration, our results indicate lower values of S_1 in the presence of **1**. This suggests that the CaI_2 ion-pairs in the absence of the receptor have a higher dipole moment than the receptor-bound ion-pairs, i.e. the I-Ca-I angle is straighter for ion-pairs bound to **1** as compared to ion-pairs in the absence of **1**.

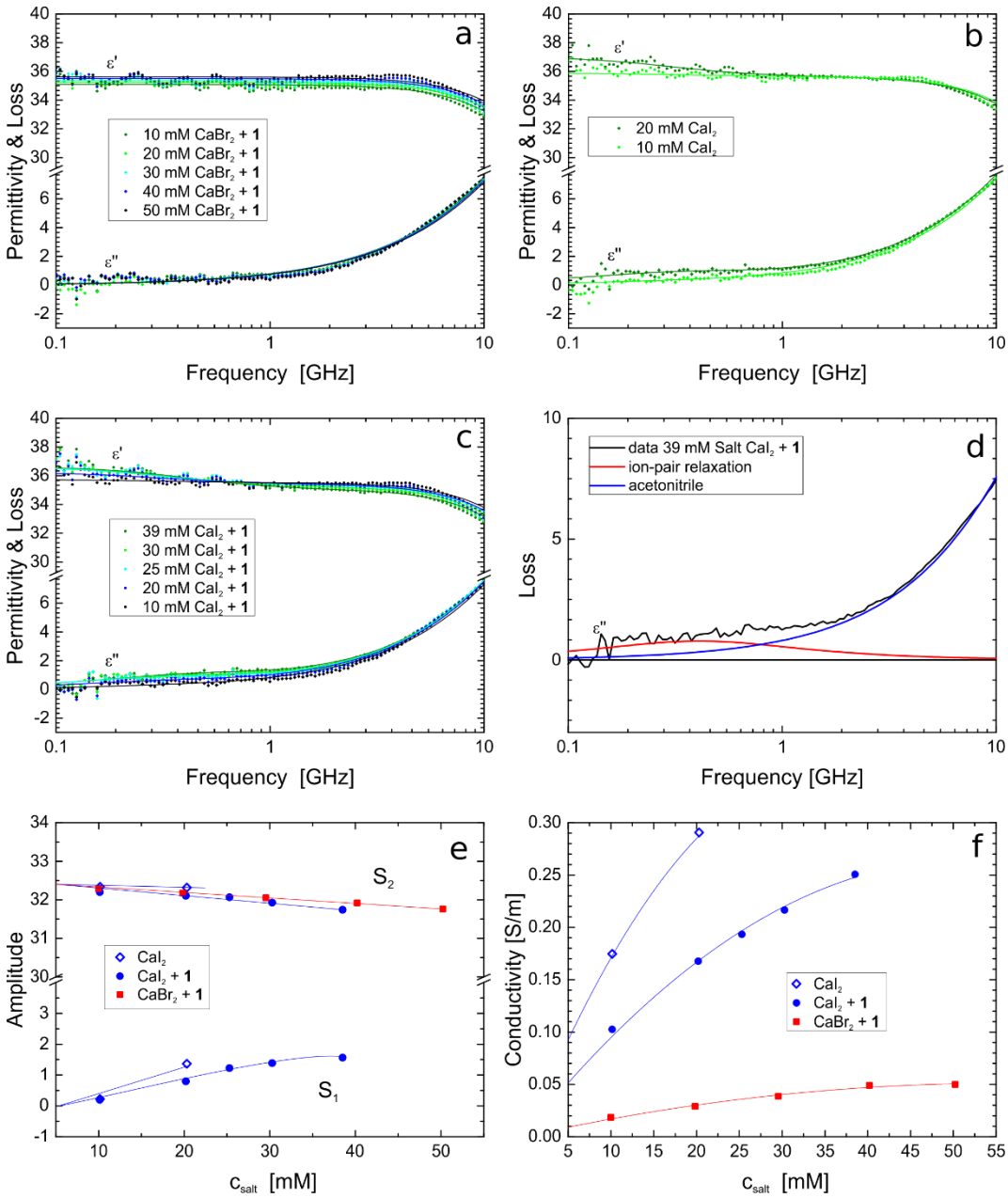

Figure S30. Dielectric permittivity spectra for solutions of (**a**) $CaBr_2$ + **1**, (**b**) CaI_2, and (**c**) CaI_2 + **1** in acetonitrile. Symbols show experimental data, and lines show fits of eq S1 to the data. In panel (**d**) the loss spectra for the 39 mM CaI_2 + **1** sample (black line) are shown together with the contribution of the lower-frequency relaxation (first term of eq S1, red line) and the acetonitrile relaxation (second term of eq S1) to the dielectric loss. Note that for visual clarity the Ohmic loss term (last term of eq S1) has been subtracted in panels (**a-d**). Panel (**e**) shows the relaxation amplitudes and panel (**f**) the conductivities as obtained from fitting eq S1 to the experimental data.

13. Copies of ^{1}H and ^{13}C NMR Spectra

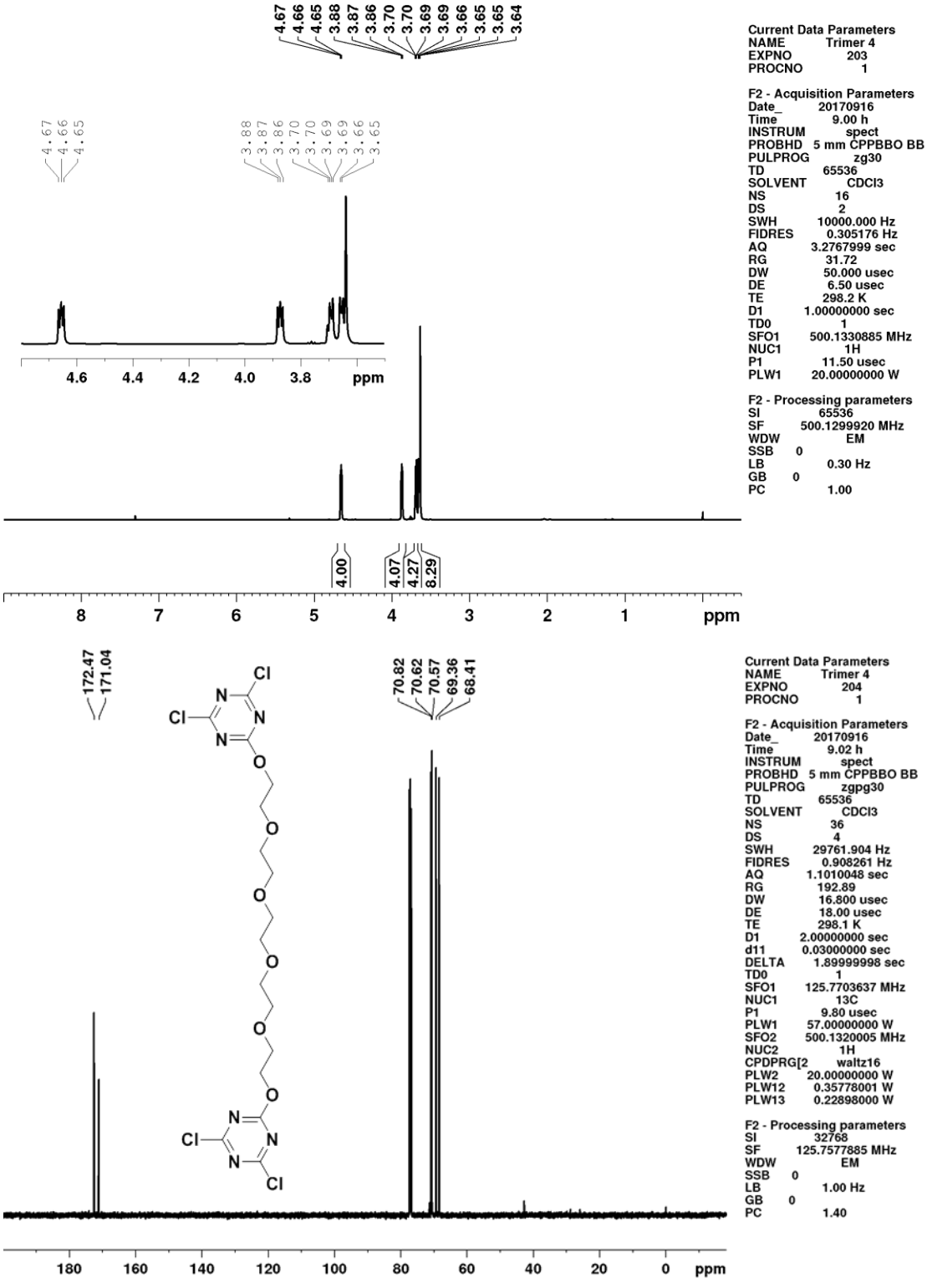

Figure S31. ^{1}H NMR ($CDCl_3$, 298 K) and ^{13}C NMR ($CDCl_3$, 298 K) Spectra of **5**.

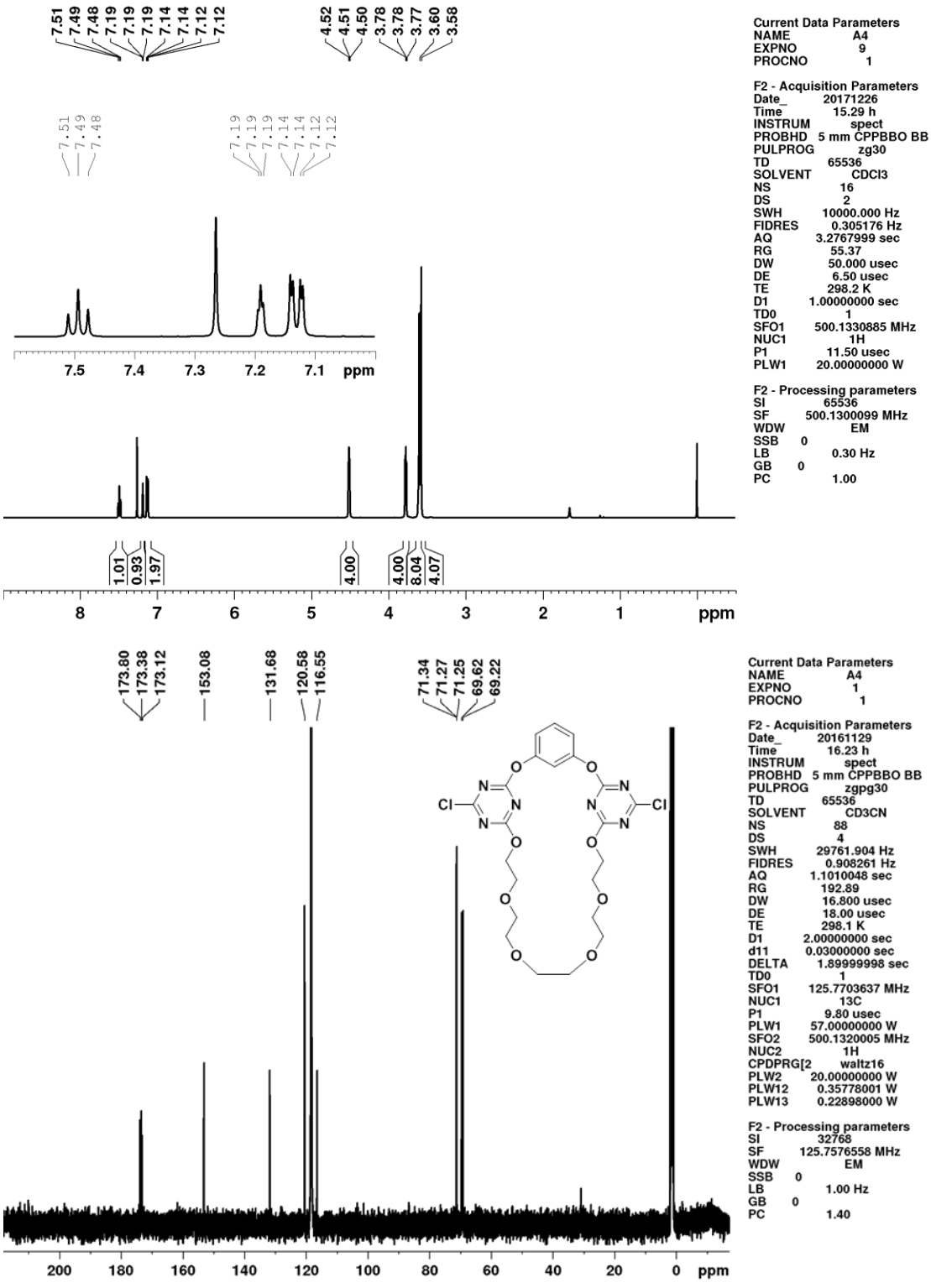

Figure S32. ^{1}H NMR ($CDCl_3$, 298 K) and ^{13}C NMR (CD_3CN, 298 K) Spectra of **1**.

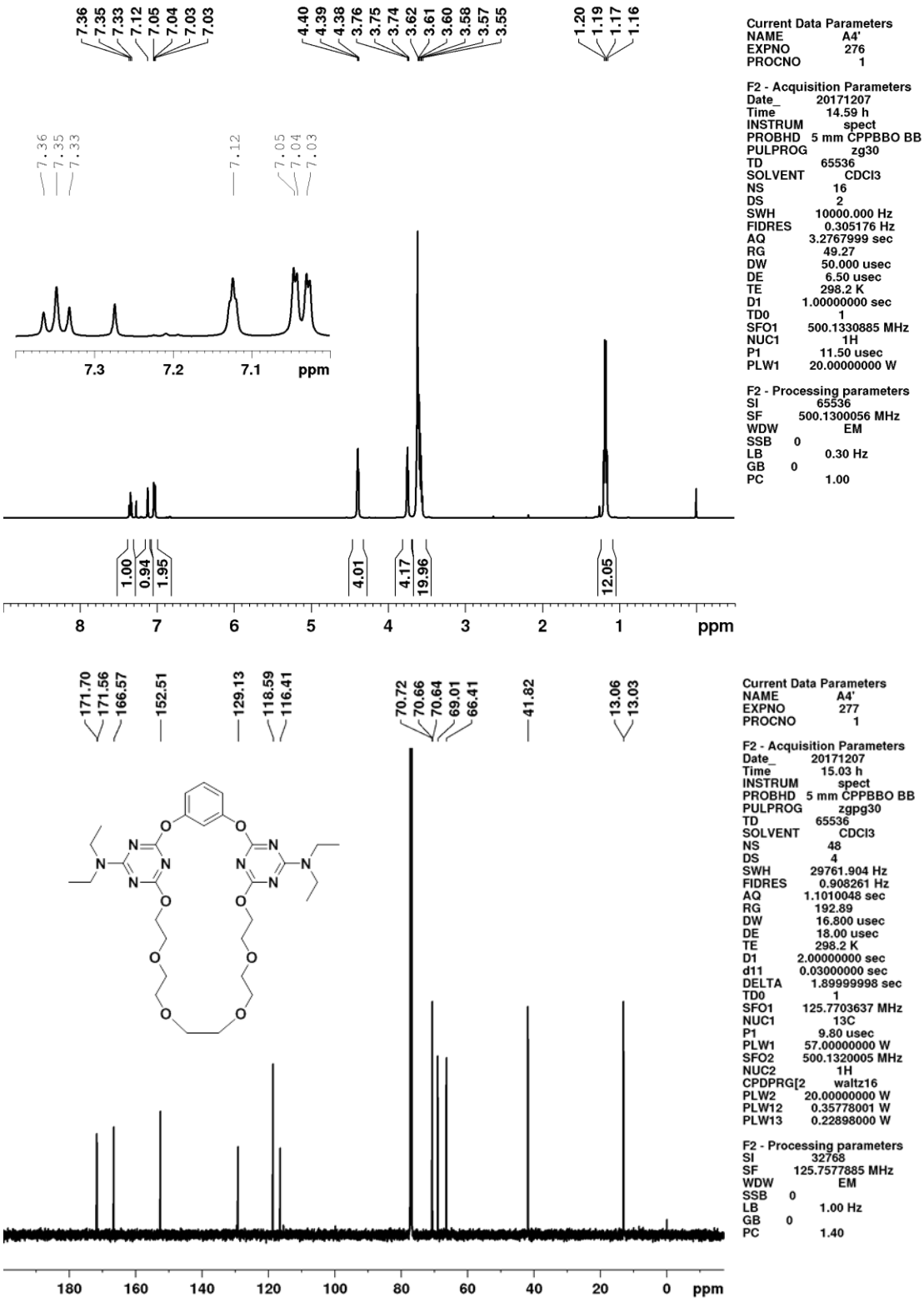

Figure S33. ^{1}H NMR ($CDCl_3$, 298 K) and ^{13}C NMR ($CDCl_3$, 298 K) Spectra of **2**.

14. References

[S1] For details concerning the way the program works see: Frassineti, C.; Ghelli, S.; Gans, P.; Sabatini, A.; Moruzzi, M. S.; Vacca, A. *Anal. Biochem.* **1995**, *231*, 374-382. Frassineti, C.; Alderighi, L.; Gans, P.; Sabatini, A.; Vacca, A.; Ghelli, S. Anal. Bioanal. Chem. **2003**, *376*, 1041.

[S2] W. Ensing, J. Hunger, N. Ottosson, H. J. Bakker, *J. Phys. Chem. C* **2013**, *117*, 12930–12935.

[S3] F. Neese, *WIREs Comput. Mol. Sci.* **2012**, *2*, 73–78.

[S4] F. Weigend, R. Ahlrichs, *Phys. Chem. Chem. Phys.* **2005**, *7*, 3297–3305.

[S5] F. Weigend, *Phys. Chem. Chem. Phys.* **2006**, *8*, 1057.

[S6] K. A. Peterson, D. Figgen, E. Goll, H. Stoll, M. Dolg, *J. Chem. Phys.* **2003**, *119*, 11113–11123.

[S7] F. Neese, *J. Comput. Chem.* **2003**, *24*, 1740–7.

[S8] O. Vahtras, J. Almlöf, M. W. Feyereisen, *Chem. Phys. Lett.* **1993**, *213*, 514–518.

[S9] S. Sinnecker, A. Rajendran, A. Klamt, M. Diedenhofen, F. Neese, *J. Phys. Chem. A* **2006**, *110*, 2235–45.

[S10] J. Hunger, A. Stoppa, A. Thoman, M. Walther, R. Buchner, *Chem. Phys. Lett.* **2009**, *471*, 85–91.

[S11] A. Stoppa, A. Nazet, R. Buchner, A. Thoman, M. Walther, *J. Mol. Liq.* **2015**, *212*, 963–968.

[S12] R. Buchner, G. Hefter, *Phys. Chem. Chem. Phys.* **2009**, *11*, 8984–99.

[S13] V. Balos, H. Kim, M. Bonn, J. Hunger, *Angew. Chemie Int. Ed.* **2016**, *55*, 8125–8128.